# Supporting Information for **"On the relationship between excited state lifetime and isomerization quantum yield in animal rhodopsins: beyond the one-dimensional Landau-Zener model"**

*Mohsen M. T. El-Tahawy[a,b,§], Artur Nenov[a,§], Oliver Weingart[c], Massimo Olivucci[d,e,*], Marco Garavelli[a,*].*

## Contents

# 1 Definitions

Here we report the definitions of terms mentioned in the main text.

Quantum yield (QY): is defined as the ratio between the trajectories reaching bathoRh over the total number of trajectories; Lifetime τ: defined as the time period it takes for half of the population to decay to the GS; Decay window: defined as twice the standard deviation of hopping events times; The average electronic population: defined as the sum of squared coefficients of each state; The trajectory occupation: defined as the ratio of trajectories in each state; The time of transition of the GS wavefunction from CT to covalent: defined as the time when the total charge on the N-terminus ($C_{12}$—N segment) reaches +0.9 e; Decision events: defined as the time step at which the charge at the N-terminus has grown to +0.9 e, indicating a completed transition of the GS wavefunction from CT to covalent; the total charge on the N-terminus: defined as the sum of all Mulliken charges in the $C_{12}$...N segment. Bond length alternation (BLA) defined as the difference between the average single-bond and the average double-bond and it is given as:

**BLA**

$$= \frac{C_6C_7 + C_8C_9 + C_{10}C_{11} + C_{12}C_{13} + C_{14}C_{15}}{5} - \frac{C_5C_6 + C_7C_8 + C_9C_{10} + C_{11}C_{12} + C_{13}C_{14} + C_{15}N}{6}$$

# 2 Methodology and Benchmarking

## 2.1 Three Pigments Models

One of the prerequisites of our computational study is the construction of a computer model starting from the crystal structure of the three pigments. In contrast to both Rh and sqRh, there is no available crystallographic data for hMeOp. Therefore, Rinaldi et. al. have exploited the high sequence similarity between sqRh, whose crystal structure is available (PDB code: 2Z73)[1], and hMeOp (40%) to construct an atomistic structural model of hMeOp (Figure S1). Here we employ the same models used in the study of Rinaldi et al. for the three pigments[2]. Briefly, the QM/MM models of Rh and sqRh were prepared utilizing only one unit of the dimeric crystallographic structures (chain A) in which all the crystallographic water molecules were included while the membrane lipids at the protein surface were excluded (for Rh: PDB code 1U19[3], resolution 2.2 Å; for sqRh: PDB code 2Z73[1], resolution 2.5 Å). On the other hand, the QM/MM model of hMeOp was constructed by homology modeling, i.e. starting from the crystallographic structure of sqRh as a template in which the retinal chromophore coordinates were kept fixed as in sqRh. This protocol of comparative modeling was validated by

reproducing the observed absorption maximum for the human rhodopsin using the crystallographic structure of bovine Rh (95% sequence similarity) as a template[2].

## 2.2 QM/MM Partitioning Scheme

The QM/MM approach has been extensively used for modeling RPSBs in solution and in proteins[2,4-8]. Our QM/MM models for the three rhodopsins are based on an high-medium-low QM/MM scheme in which the QM/MM boundary was placed on the Lys Cδ–Cε bond and the link–atom approach was used to model the frontier (Figure S2)[9-11]. The whole PRSB chromophore is treated quantum mechanically (54 atoms including the link atom) keeping the protein environments fixed at their crystal structure atomic positions except the closest 9 atoms of the lysine side–chain connected to the PRSB were free to move (i.e., as M layer). The protein environments were described by a modified AMBER96 force field. Electrostatic embedding was used to describe the interaction between MM and QM systems[6].

**Figure S1**. Comparative model (violet) of hMeOp superimposed on top of sqRh crystallographic structure used as template (green), this Figure taken from ref[2].

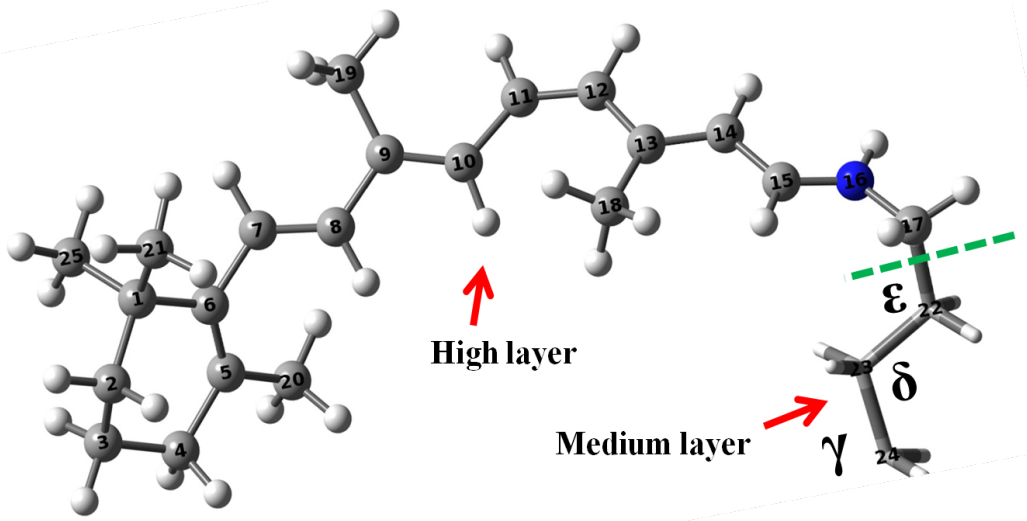


**Figure S2.** Schematic representation for high and medium layers, the green dashed line shows the cut between the H and M layers. The atoms in ball and stick representations belong to the QM region while atoms represented as tubes belong to the medium layer. The low layer includes the rest of the protein not shown in the figure.

## 2.3 Optimization and Single Point Calculations

The ground state structures of the three pigments were optimized at the complete active space self–consistent field CASSCF/6–31G*/AMBER level with single root employing CAS (10,10) and CAS(12,12) active spaces (see next section). The CASSCF calculation was followed by subsequent multiconfigurational second–order perturbation theory (CASPT2) computations to estimate the dynamic correlation energy of each state in order to get a more quantitative evaluation of the excitation energies as well as generate the linear absorption spectra and to estimate the relaxed scan along the CCCC coordinate[12]. This combined CASPT2//CASSCF approach has been shown to return experimentally accurate energies with errors within 0.2-0.3 eV[13-14]. An imaginary level–shift of 0.2 au was used to decrease the influence of weakly interacting intruder states in the CASPT2 calculations[15]. The ionization potential and electron affinity parameter was set to 0.0 au[16], in accordance with previous studies of retinal in gas–phase and its protein environment[13, 17-19].

## 2.4 Selecting the Active Space

The complete active space CAS(12,12) of RPSB comprises twelve electrons in twelve π–orbitals (Figure S3), yet such a large active space may be practically used for optimization but it is impractical for frequency calculations and extensive dynamics simulations. A possible way to overcome this problem is to reduce the active space to ten electrons in ten π–orbitals CAS(10,10) by rejecting one occupied and one virtual π–orbitals from the full π–system. In order to select the two orbitals that have the least pronounced effect on the results we have computed for each pigment a single adiabatic trajectory with zero initial velocity (i.e. 0K reference trajectory) employing both the full-π CAS(12,12) and the a reduced active space CAS(10,10). For this purpose, many trials have been performed, each time excluding a couple of π/π*–orbitals (i.e. one occupied and one virtual). Eventually, the reduced active space that most accurately reproduced the reference CAS(12,12) trajectories was selected for running systematic dynamical studies.

We found that the trajectories computed with a CAS(10,10 excluding the pair of bonding and non-bonding π-orbitals localized on the β-ionone ring (Figure S3) reproduced perfectly both the energy profiles and the structural features shown using the full-π CAS(12,12) active space along the whole photoisomerization path (see Figure S4 and Figure S5). The resulting orbital set was therefore used for dynamics computations.

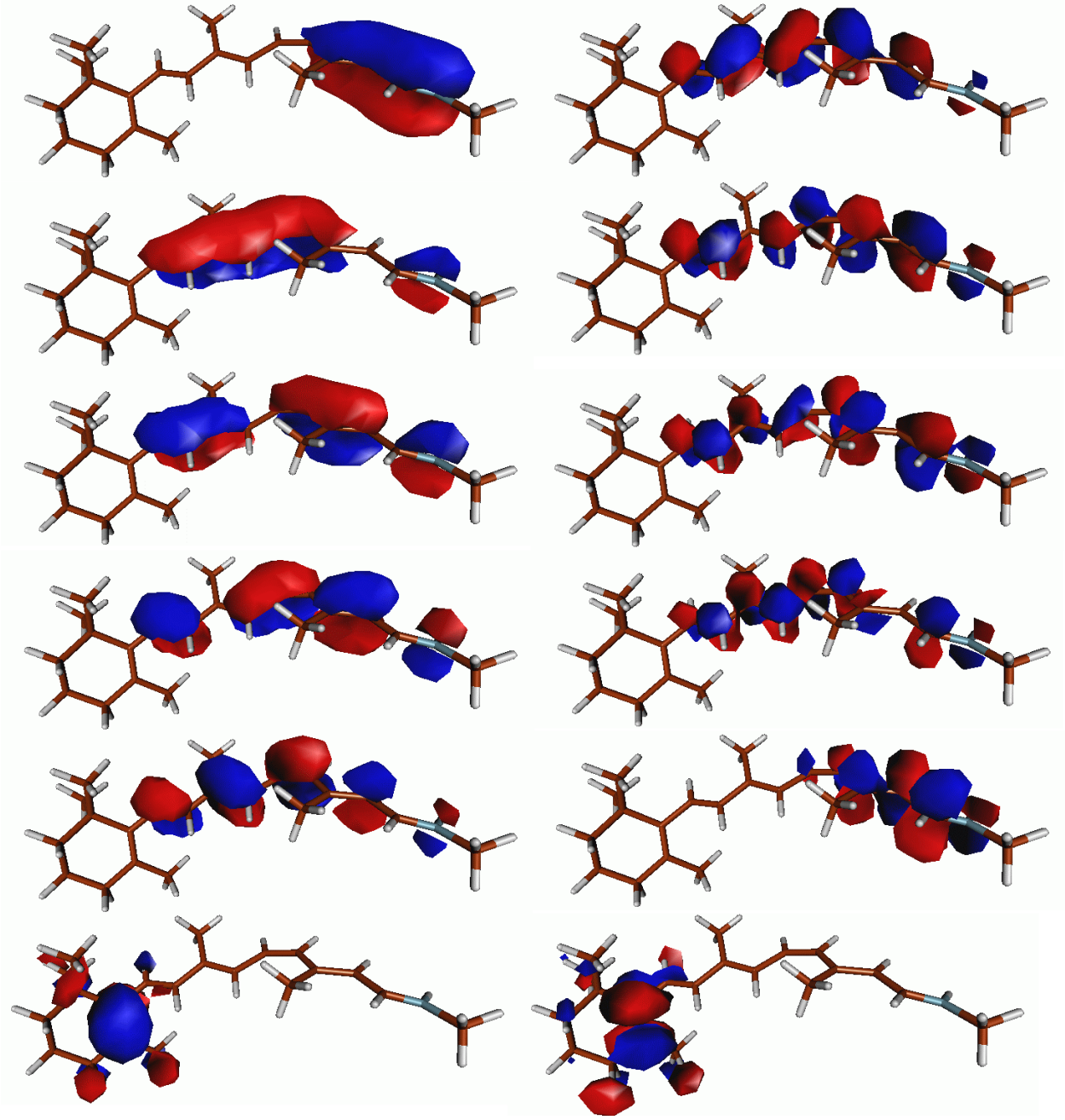

**Figure S3**. The molecular orbitals comprising the full active space CAS(12,12). Highlighted in gray is the neglected pair of bonding and anti-bonding orbitals resulting in the reduced CAS(10,10) which best reproduces the energy profiles and the structural features obtained using the full-π active space.

## 2.5 MD Simulations

### 2.5.1 0K Trajectories

Reference trajectories (FC trajectories) were started without any initial kinetic energy for the three pigments at the CASSCF/6–31G*/AMBER96 level using two different active spaces CAS (10,10) and CAS (12,12) starting from the corresponding optimized FC geometries. $S_1$

excited state trajectories were calculated at the same level of theory used for ground state optimization, but with state–averaging (weights: 0.5, 0.5) employing time steps of 0.5 employing both (10,10) and (12,12) active spaces. The time step was reduced to 0.25 fs in the vicinity of the crossing between $S_0$ and $S_1$ (i.e. $\Delta E_{S1\text{-}S0}$<15 kcal/mol); surface hopping was suppressed, i.e. the molecules were forced to stay in the excited state during the whole simulation.

While the agreement between computed and experimental absorption band and $\lambda_{max}$ values supports the qualitative reliability of the limited ensemble generated by the sampling procedure, one could ask if the CASSCF method, which does not account for a significant part of the dynamic electron correlation, can be used to perform semi-classical trajectory calculations correctly. This question is important when the missing dynamic electron correlation has different weights in the $S_1$ and $S_2$ states. In other words, $S_2$ and $S_1$ would be well separated and thus the ES progression would be completely driven by the $S_1$ potential energy surface, after dynamic electron correlation energy correction (i.e. after re-computing the energy profiles at the SS-CASPT2 or MS-CASPT2 levels) while at the CASSCF level the $S_2$ state may mix with $S_1$ and seriously interfere with the $S_1$ motion.

In order to provide evidence that this potential issue is not significantly affect the presented results, we have computed and analyzed three QM/MM semi-classical trajectories (also called FC trajectories) which were calculated by starting at the corresponding FC points on the $S_1$ energy surface without initial velocities and propagating until reaching the $S_1/S_0$ intersection seam (the same trajectories were presented in ref.[2]). In principle, such trajectories follow the minimum energy path along the ES potential energy surface and are assumed to provide information on the dynamics of the center of the excited state population (i.e. the vibrational wavepacket) projected on the ES upon excitation[20]. The analysis of the Rh, sqRh and hMeOp FC trajectories shows that the $S_2/S_1$ mixing is noticeable only in the FC region and last just few fs. In other words, within 10 fs the electronic structure of the $S_1$ state acquires a pure charge transfer character in all systems consistently with previous works on Rh[2, 21], Figures S4 and S5.

We conclude that the only change resulting from the SS-CASPT2 or MS-CASPT2 corrections is a decrease in the slope of the $S_1$ potential energy surface connecting the FC point to the CI. As elaborated previously such change translates in a proportionality in the resulting energy gradients and, finally, in a scaling factor to the simulation time[2, 21] but it should not affect

the qualitative outcome of the comparison. On this basis, we assume that the trends in ES lifetimes and QYs will not change when using the CASSCF force field.

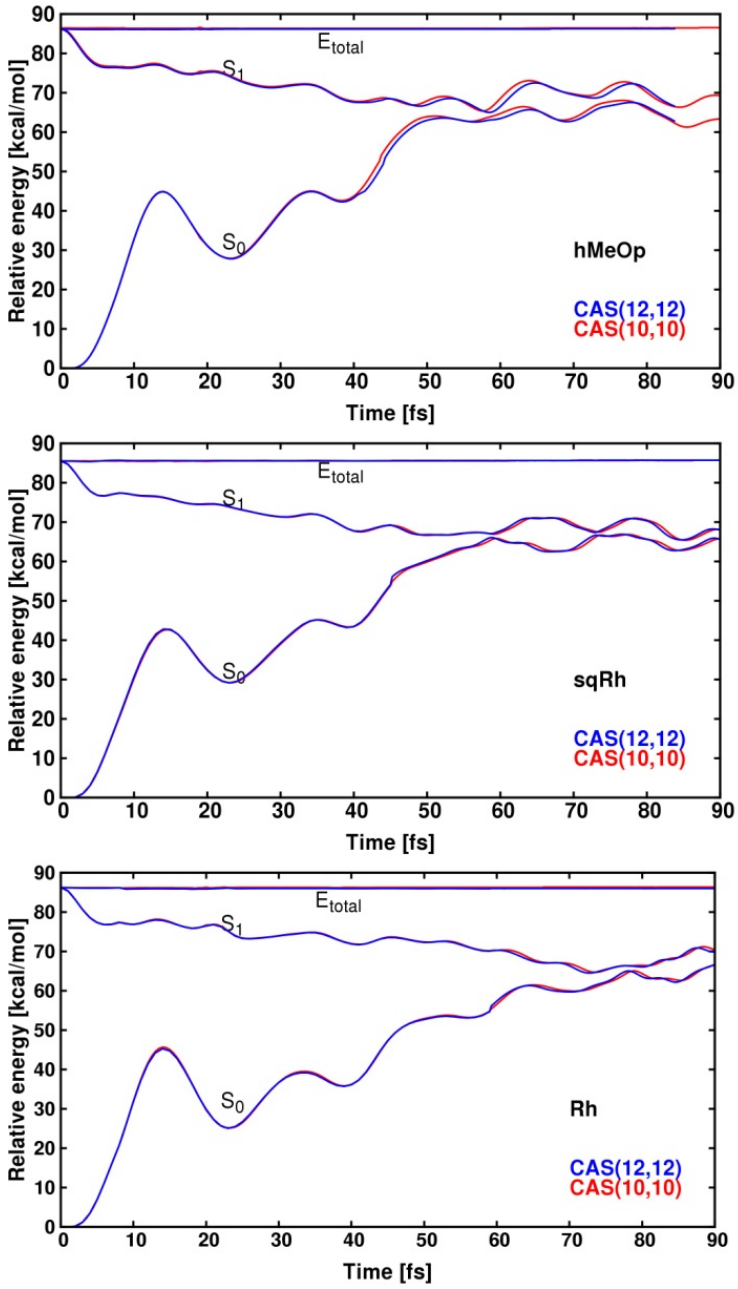


**Figure S4.** Overlay of $S_1$ and $S_0$ and total energies in pigment trajectories computed with CAS (10,10) and CAS (12,12) active spaces shown in red and blue colours, respectively. The CAS space has virtually no influence on the excited state dynamics.

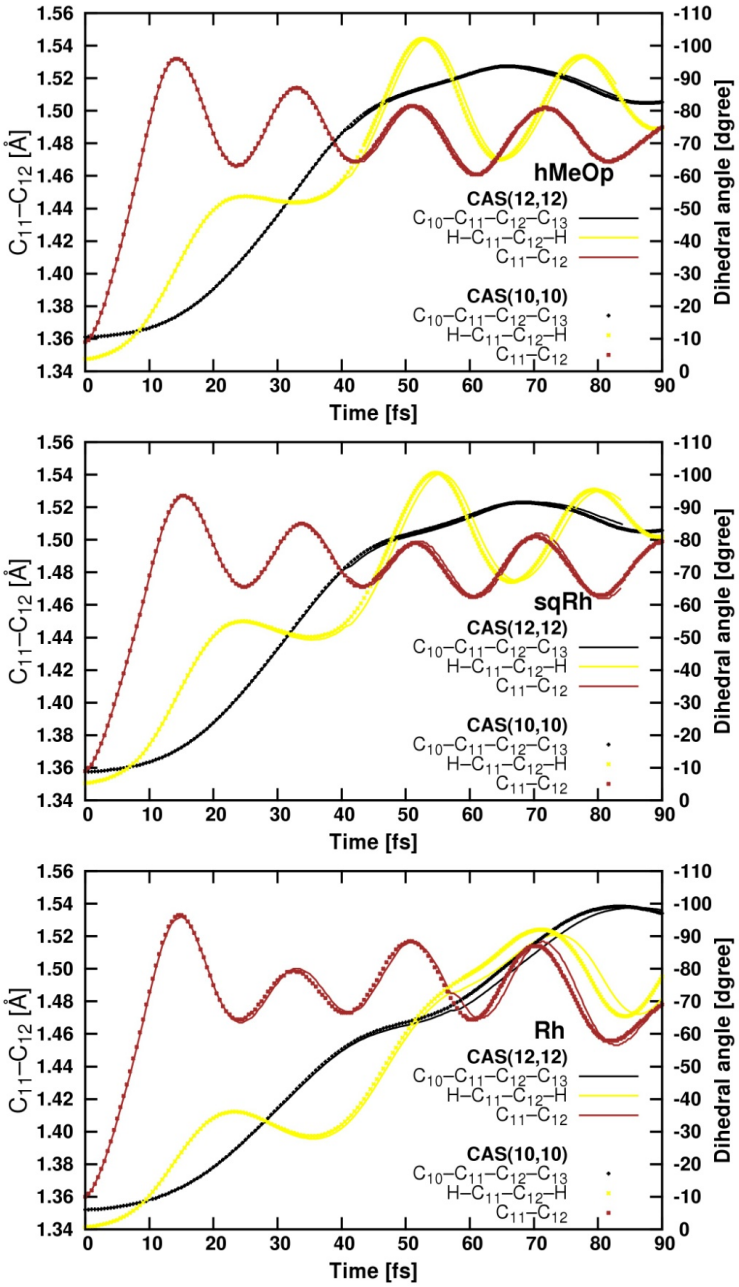


**Figure S5.** Overlays of $C_{11}$–$C_{12}$ bond length, $C_{10}$–$C_{11}$–$C_{12}$–$C_{13}$ and H–$C_{11}$–$C_{12}$–H dihedrals in 0K trajectories computed with CAS(10,10) (dashed lines) and CAS(12,12) (solid lines) active spaces.

### 2.5.2 Trajectory Swarms

On the basis of the demonstrated similarity of the results of the 0K trajectories produced with the two active spaces, CAS (10,10) was employed for the computation of the room temperature trajectory swarms. For each pigment, numerical frequencies were calculated on top of the re–optimized ground state CASSCF(10,10)/6–31G* geometries. A set of 60 geometries with their associated velocities were created using thermal sampling option as implemented in Gaussian 03[22] at a temperature of 300K. This routine considers the zero-point energy and additional temperature effects by exciting the vibrational modes according to

Boltzmann statistics. Such set of initial conditions is intended to mimic the wave packet nature of the quantum-mechanical system. The molecular dynamics simulations were started in the bright excited state ($S_1$) employing a two root state averaged CAS(10,10)/6-31G* description and a time step of 0.5 fs. The time step was reduced to 0.25 fs in the vicinity of a crossing (i.e. $\Delta E_{S1\text{-}S0}$<15 kcal/mol). Trajectories were propagated with a velocity Verlet algorithm at constant total energy[23]. The surface hop between $S_1$ and $S_0$ potential energy surfaces was activated: a Tully's fewest switches surface hopping algorithm with decoherence correction (d = 0.1 au)[24] was used for this purpose. Back hopping to the ground state was suppressed during simulation. Trajectories were computed up to the formation of clear ground state photoproducts through tracking the evolution of the $C_{10}$–$C_{11}$–$C_{12}$–$C_{13}$ torsion angle. The molecular orbitals calculated using MOLCAS 7[23] were transformed to MOLPRO 2009[9,25] in order to calculate the non-adiabtic coupling vectors. All QM/MM single point, geometry optimizations, numerical frequency and molecular dynamic calculations have been performed using COBRAMM, a QM/MM program interfacing various QM and MM codes[8,25-27].

## 2.6 Time Scaling of the Excited–State Trajectory

It is well established that the missing dynamical correlation at the CASSCF level may affect significantly the energy profiles and thus the resulting non-adiabatic dynamics. This may result in erroneous state ordering, different potential energy surface topography, variations in activation barriers, topology of conical intersections, etc. In ref.[21] Olivucci and co-workers showed that under the assumption of a linear relation between the CASSCF and CASPT2 energies, CASPT2 corrected time scales and energy profiles can be obtained. This assumes that that the energies are related via a proportional factor α according to the relation:

$$\boldsymbol{\alpha E_{CASSCF}(x) = E_{CASPT2}(x)} \quad \mathbf{(1)}$$

The factor $\boldsymbol{\alpha}$ in the energies translates into a proportionality in the resulting energy gradients. Furthermore, the authors showed that the linear relation holds for Rh by exploring the minimum energy path at CASSCF and CASPT2 levels. They demonstrated that the uncorrelated CASSCF energy profile is steeper than the correlated CASPT2 profile, resulting in α values < 1.0, and, hence, smaller gradients. Furthermore, they argued that since the molecular dynamics explores a region of the PES that is close to the reaction path, one may assume that this relation is also valid along any computed trajectory. As the gradient enters in the Velocity-Verlet algorithm as the system's acceleration during the molecular dynamics its scaling has an immediate effect on the simulation's time:

$$t_{scaled} = t_{unscaled}\alpha^{\frac{1}{2}} \quad (2)$$

where $t_{unscaled}$ is the "unphysical" time resulting from the CASSCF dynamics, and $t_{scaled}$ is the scaled "physical" time that would be obtained if the dynamics would have been run at the CASPT2 level. Assuming that the same linear relation α, holds also in the pigments investigated in this study we have calculated the CASPT2 and CASSCF excited–state energies along the reaction path from the relaxed FC region to the conical intersection with the ground state by means of a relaxed scan around $C_{10}$-$C_{11}$-$C_{12}$-$C_{13}$ torsional coordinate with 10° increment. The values for the parameter α were then obtained by linear fitting of the corresponding energies of $S_0$, $S_1$ and ΔE (Figure S6, S7 and Table S1). The linear relation for all three pigments holds well in the explored region ($R^2$ value of 0.99) giving an averaged scaling factor α~0.81 for all three pigments being consistent with the previously reported Rh value (0.795) based on fitting the energy of the $S_1$ state[21].

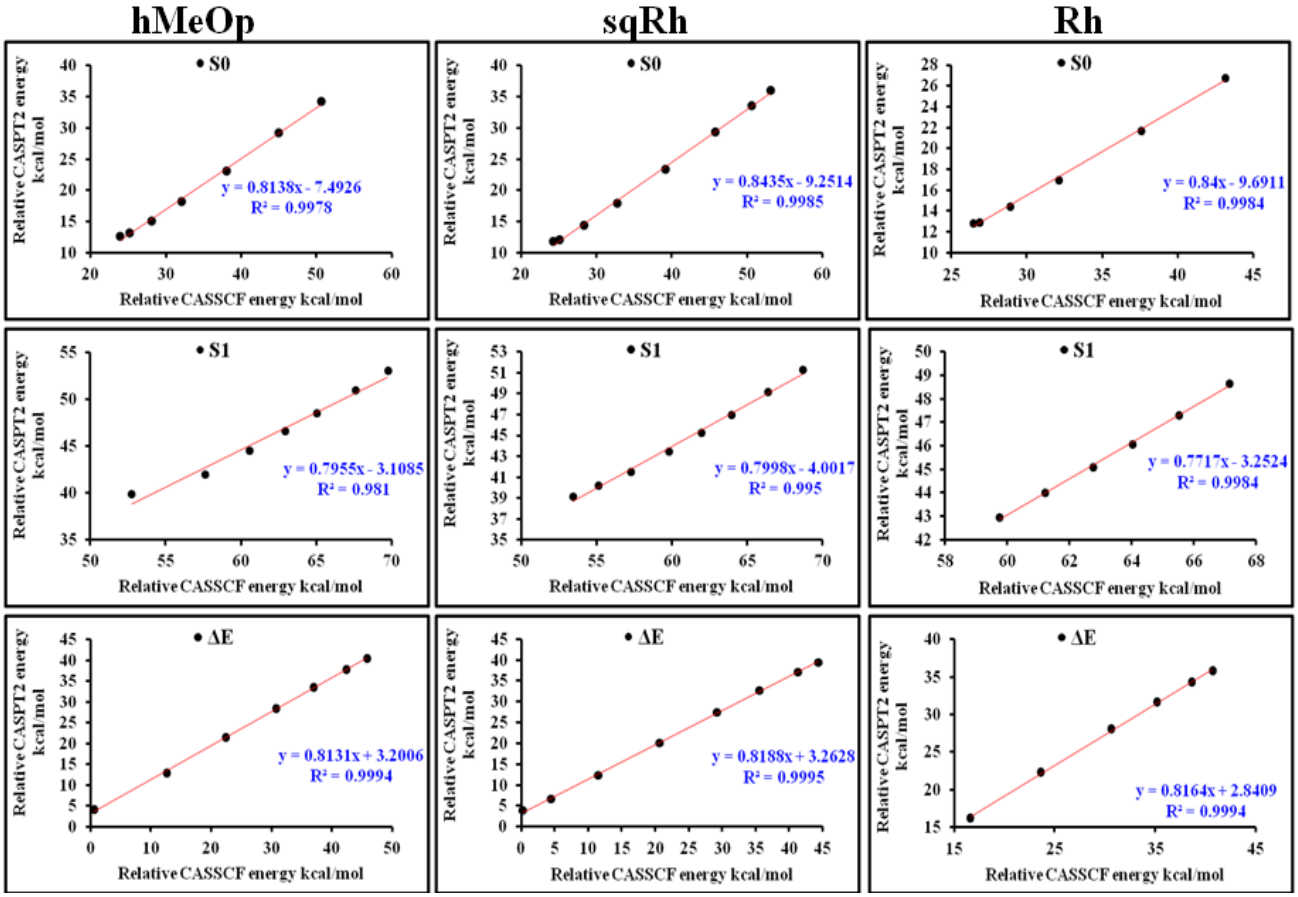


**Figure S6.** Linear fit of relative energies (referred to the ground–state minimum) calculated at CASPT2 and CASSCF level of theory along the computed CASSCF reaction path.

**Table S1**. α values according the linear fitting between CASSCF and CASPT2 of $S_0$, $S_1$ and ΔE energies

| | $S_0$ | $S_1$ | ΔE | Average |
|---|---|---|---|---|
| **hMeOp** | 0.8138 | 0.7955 | 0.8131 | 0.811 |
| **sqRh** | 0.8435 | 0.7998 | 0.8188 | 0.832 |
| **Rh** | 0.8400 | 0.7717 | 0.8164 | 0.798 |

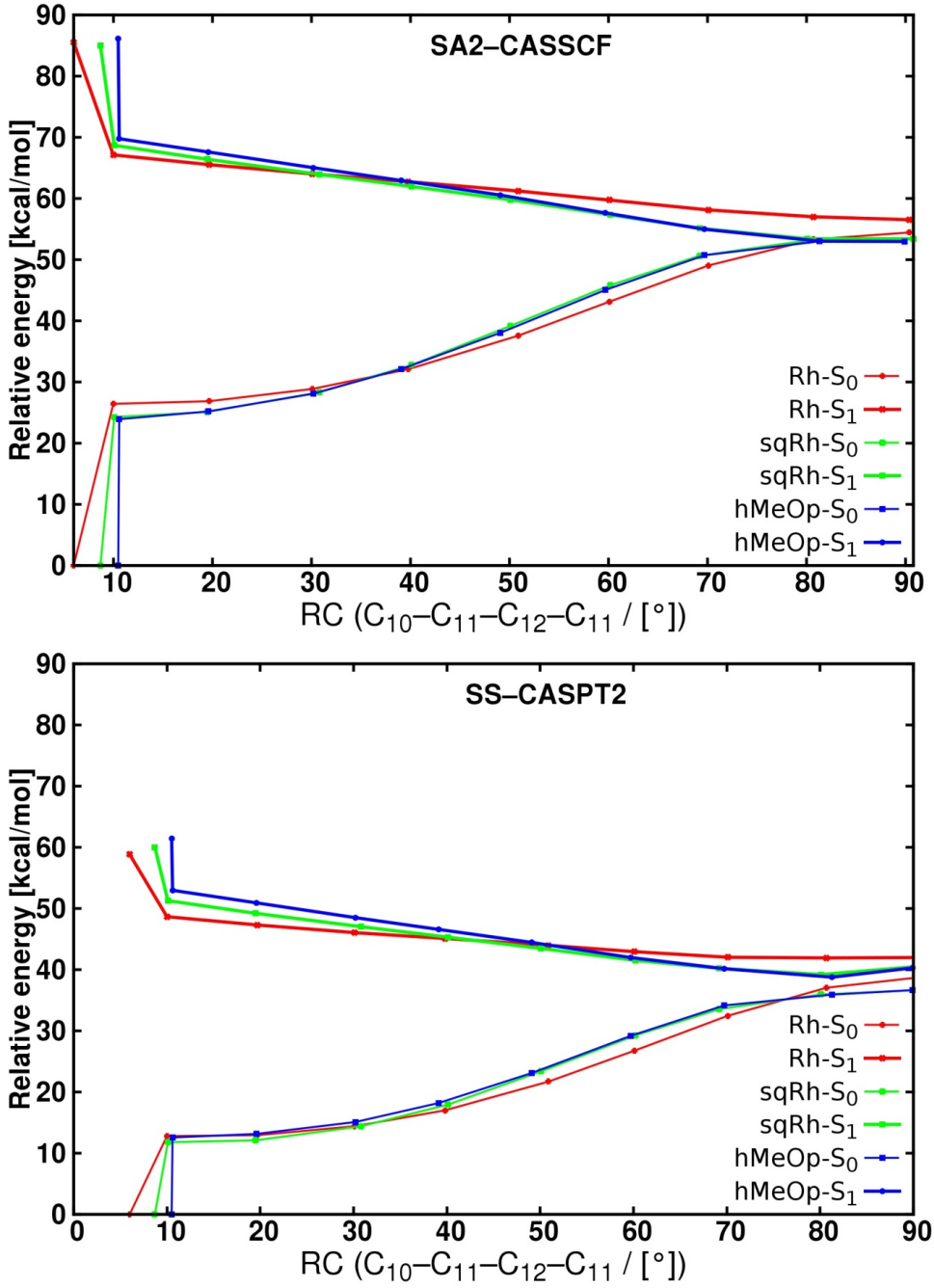


**Figure S7**. SA2–CASSCF(12,12)6–31G*/AMBER and SS-CASPT2 energy profiles along the torsion angle $C_{10}$–$C_{11}$–$C_{12}$–$C_{13}$ obtained from constrained relaxed scan with 10° increment.

## 3 Geometrical and Electronic Structures of the models

The constructed QM/MM models reproduce the results of Rinaldi et al.[2] and is here briefly summarized**.** The $S_0$ equilibrium structures show a similar BLA positive value of ca. 0.12 Å corresponding to a clear alternating single-double bond pattern with limited delocalization. The cavity embedding distorts the conjugated chain out-of-plane with respect to the gas-phase equilibrium structure of rPSB11. In fact, we observe a progressive increase of the CCCC dihedral in the series Rh (-6°)→sqRh (-9°)→hMeOp (-11°), as well as a notable -17° (Rh), -23° (sqRh) and -19° (hMeOp) deviation from planarity of the $C_{11}$-$C_{12}$–$C_{13}$-$C_{14}$ dihedral describing the twisting about the single bond adjacent to the reactive $C_{11}$-$C_{12}$ double bond. In contrast, the β–ionone ring exhibits a less pronounced twisting with respect to the gas-phase rPSB11 equilibrium structure (-66°), with hMeOp and sqRh displaying values of ca. -60° and Rh displaying a value of ca. -55° (Table S2).

In all cases, the $S_0$→$S_1$ vertical excitation corresponds to a bright state (i.e. it features a large oscillator strength) with a dominant contribution of the HOMO→LUMO (see Figure S3) transition resulting in a $S_1$ state with charge transfer character with respect to the $S_0$ which is covalent. By covalent character we refer to the usual covalent bonding where the electrons forming the π-component of the –$C_{11}$-$C_{12}$– double bond reside on $C_{11}$ and $C_{12}$ and are single spin coupled. This differs from the charge transfer character of –$C_{11}$(+)–$C_{12}$= type[28]. In contrast, $S_0$→$S_2$ is dominated by the HOMO→LUMO double excitation and HOMO-1→LUMO single excitation and has limited oscillator strength consistent with a dominant open-shell diradical character. The computed vertical excitation energies reproduce, when converted in wavelength values, the trend of observed absorption maxima ($\lambda_{max}$) with Rh featuring a red-shifted $\lambda_{max}$ with respect to sqRh and hMeOp which have 1 and 2 kcal/mol larger excitation energies (Table S3), respectively (notice that, all computed excitation energies are, systematically blue-shifted by ca. 2 kcal/mol[2] with respect to the experimental quantities[29-31]).

As already established for Rh[32-34], $\lambda_{max}$ values are determined by the non-uniform electric field generated by the protein cavity. In the studied pigments the electrostatic interaction introduces a blue-shifting effect of ca. 8 kcal/mol for hMeOp and sqRh and 7 kcal/mol for Rh (SS-CASPT2 level). In hMeOp and in sqRh the effect is dominated by E215 and E172 which change the excitation energy by ca. 5 and 9 kcal/mol, respectively, when set to zero. These E215 and E172 residues are homologous to the E181 secondary counterion of Rh, which has

only a small effect on excitation energy. In fact, the excitation energy in Rh is dominated (ca. 18 kcal/mol blue-shifting effect) by the interaction with the E113 primary counterion[2], see Ref. 2 for the effect of the other restudies.

The conformational distortion of rPSB11 induced by the different protein cavities also influences the $\lambda_{max}$. In fact, the excitation energy trend displayed by the three rhodopsins is retained in the corresponding chromophores when these are extracted from their protein cavities (or equivalently, when all protein charges are set to zero). This behavior, can be correlated to the progressive increase of the CCCC value (see above).

**Table S2**. The ground state geometrical parameters optimized using CAS(12,12) and CAS(10,10) active spaces

| | CAS(12,12) | | | | CAS(10,10) | | |
|---|---|---|---|---|---|---|---|
| **Parameter \| Moodel** | **Rh** | **sqRh** | **hMeOp** | **Vac.** | **Rh** | **sqRh** | **hMeOp** |
| **$C_5$–$C_6$** | 1.352 | 1.351 | 1.354 | 1.353 | 1.332 | 1.332 | 1.334 |
| **$C_6$–$C_7$** | 1.493 | 1.491 | 1.494 | 1.493 | 1.494 | 1.491 | 1.495 |
| **$C_7$–$C_8$** | 1.352 | 1.346 | 1.348 | 1.349 | 1.351 | 1.347 | 1.348 |
| **$C_8$–$C_9$** | 1.474 | 1.469 | 1.471 | 1.471 | 1.474 | 1.470 | 1.472 |
| **$C_9$–$C_{10}$** | 1.361 | 1.359 | 1.360 | 1.364 | 1.361 | 1.359 | 1.360 |
| **$C_{10}$–$C_{11}$** | 1.464 | 1.459 | 1.459 | 1.451 | 1.465 | 1.459 | 1.459 |
| **$C_{11}$–$C_{12}$** | 1.360 | 1.358 | 1.357 | 1.363 | 1.360 | 1.358 | 1.357 |
| **$C_{12}$–$C_{13}$** | 1.466 | 1.471 | 1.467 | 1.460 | 1.466 | 1.471 | 1.467 |
| **$C_{13}$–$C_{14}$** | 1.370 | 1.364 | 1.365 | 1.370 | 1.370 | 1.364 | 1.365 |
| **$C_{14}$–$C_{15}$** | 1.434 | 1.425 | 1.429 | 1.428 | 1.435 | 1.425 | 1.429 |
| **$C_{15}$–$N_{16}$** | 1.292 | 1.294 | 1.293 | 1.292 | 1.292 | 1.294 | 1.293 |
| **$C_5$–$C_6$–$C_7$–$C_8$** | –54.9 | –61.6 | –60.7 | –65.7 | –55.4 | –62.8 | –61.9 |
| **$C_6$–$C_7$–$C_8$–$C_9$** | 179.3 | –177.6– | 178.7 | –178.6 | 179.3 | –177.4 | 178.8 |
| **$C_7$–$C_8$–$C_9$–$C_{10}$** | –173.5 | 176.0 | 171.2 | 179.5 | –172.4 | 176.3 | 171.2 |
| **$C_8$–$C_9$–$C_{10}$–$C_{11}$** | 173.9 | 177.9 | 178.0 | 179.9 | 173.8 | 178.0 | 178.0 |
| **$C_9$–$C_{10}$–$_{C11}$–$C_{12}$** | 163.1 | 165.1 | 164.6 | 176.4 | 163.3 | 165.0 | 164.5 |
| **$C_{10}$–$C_{11}$–$C_{12}$–$C_{13}$** | –6.0 | –8.8 | –10.6 | –2.7 | –6.0 | –8.7 | –10.5 |
| **$C_{11}$–$C_{12}$–$C_{13}$–$C_{14}$** | 163.0 | 156.6 | 161.0 | 175.7 | 163.1 | 156.5 | 160.9 |
| **$C_{12}$–$C_{13}$–$C_{14}$–$C_{15}$** | –178.3 | 179.0 | 172.8 | –179.8 | –178.3 | 179.1 | 172.8 |
| **$C_{13}$–$C_{14}$–$C_{15}$–N** | 168.4 | 168.0 | 169.1 | 179.1 | 168.4 | 167.8 | 169.2 |
| **H–$C_{11}$–$C_{12}$–H** | –0.7 | –5.3 | –3.8 | –1.1 | –0.7 | –5.3 | –3.8 |
| **$C_8$–$C_9$–$C_{10}$–H** | –1.9 | 0.4 | 0.6 | 0.1 | –1.9 | 0.5 | 0.6 |
| **$C_{14}$–$C_{15}$–N–H** | –1.0 | –0.3 | –3.7 | 0.0 | –0.9 | –0.4 | –3.7 |
| **$C_7$–$C_9$–$C_{10}$–H** | 177.2 | 179.1 | –179.6 | 179.8 | 177.3 | 179.1 | –179.6 |
| **BLA** | 0.12 | 0.12 | 0.12 | 0.11 | 0.12 | 0.12 | 0.12 |

**Table S3**. SS–CASPT2 and MS–CASPT2//CASSCF(12,12) and(10,10)/6–31G*/AMBER computed absorption maxima ($\lambda_{max}$, nm) and corresponding oscillator strengths f, state–averaged over three roots (weights: 1/3, 1/3, 1/3) and calculated on top of the corresponding $S_0$ minima.

| | | CAS (12,12) | | | | | | | | CAS (10,10) | | | | | | | | |
|---|---|---|---|---|---|---|---|---|---|---|---|---|---|---|---|---|---|---|
| | | SS-PT2 | | | | MS-PT2 | | | | SS-PT2 | | | | MS-PT2 | | | | exp. |
| | Model | λ1 | λ2 | f1 | f2 | λ1 | λ2 | f1 | f2 | λ1 | λ2 | f1 | f2 | λ1 | λ2 | f1 | f2 | λ1 |
| protein | hMeOp | 468 | 326 | 0.64 | 0.3 | 452 | 313 | 1.2 | 0.1 | 463 | 325 | 0.7 | 0.3 | 449 | 312 | 1.2 | 0.1 | 467–480 |
| | SqRh | 477 | 329 | 0.58 | 0.3 | 463 | 316 | 1.1 | 0.1 | 469 | 328 | 0.6 | 0.3 | 458 | 314 | 1.1 | 0.1 | 489 |
| | Rh | 486 | 332 | 0.59 | 0.3 | 469 | 313 | 1.3 | 0.1 | 475 | 329 | 0.6 | 0.3 | 462 | 310 | 1.3 | 0.1 | 498 |
| isolated | hMeOp | 538 | 340 | 0.65 | 0.3 | 505 | 331 | 1.2 | 0.2 | 526 | 337 | 0.7 | 0.3 | 497 | 328 | 1.2 | 0.2 | |
| | SqRh | 545 | 344 | 0.62 | 0.3 | 513 | 335 | 1.1 | 0.3 | 531 | 339 | 0.6 | 0.3 | 502 | 330 | 1.1 | 0.2 | |
| | Rh | 554 | 349 | 0.67 | 0.3 | 518 | 340 | 1.2 | 0.3 | 530 | 339 | 0.7 | 0.3 | 499 | 330 | 1.3 | 0.2 | |
| | Vac. | 535 | 347 | 0.82 | 0.2 | 495 | 334 | 1.5 | 0.2 | | | | | | | | | |
| | Vac.(-55) | 549 | 350 | 0.8 | 0.2 | 504 | 337 | 1.5 | 0.2 | | | | | | | | | |

## 4 Absorption Band

Figure 8 depicts the experimental (dashed lines) and simulated (solid lines) linear absorption (LA) spectra of hMeOp, sqRh and Rh. The theoretical spectra were computed using the 60 snapshots of the three RT ensembles. These points are the same employed for starting the semi-classical trajectories. The spectra consist of an intense broad unstructured band in the Visible (Vis) with a maximum between 475 nm and 500 nm, hMeOp showing the most blue-shifted band, Rh the most red-shifted. Wavefunction analysis shows that the Vis band is associated with the $S_0 \rightarrow S_1$ transition. The $S_0 \rightarrow S_2$ transition is the source of a weaker band in the near-ultraviolet around 340 nm (not shown). We observe a nearly quantitative agreement between theory and experiment for Rh and a fair agreement in the case of SqRh, where the experimental spectrum shows a somewhat steeper decrease in the red. Interestingly, compared with the SS-CASPT2 level (Figure S8 bottom-panel), MS-CASPT2 better reproduces the experimental lineshapes (Figure S8 top-panel). The simulated spectrum of hMeOp strikes as the outlier in this comparison, showing a clear undersampling in the blue and, hence, reproducing only partially the blue-shift of the absorption band with respect to SqRh. There are two possible reasons for the discrepancy: a) due to the lack of a crystal structure hMeOp simulations rely on a homology model based precisely on SqRh, hence, disagreement with the experiment could be traced back to deficiencies of the model; b) hMeOp features the closest lying (and, hence, most strongly mixing) $S_1$ and $S_2$ states. As a consequence, MS-CASPT2 causes the largest energy splitting, thereby pushing the $S_1$ state too much to the red. Overall, the trend of the $\lambda_{max}$ values in the spectra is consistent with the trend of the vertical excitation energies computed at the FC point (the former being 2-3 kcal/mol red-shifted as expected when

the absorption energy is averaged over an ensemble of geometry realizations, see Tables S3 and S4).

While the agreement between computed and experimental $\lambda_{max}$ values supports the qualitative reliability of the limited ensemble generated via the sampling procedure, it could be questioned if an inferior method like CASSCF, which is used to perform the molecular dynamics simulations, suffices to describe the pigment-specific characteristics of the electronic structure of the embedded RPSB.

In favor of the use of CASSCF we note that the ionic/covalent wavefunction mixing addressed above which requires a dynamically correlated treatment (MS-CASPT2 level) is particularly strong only in the FC region. Following its immediate departure (within 10 fs as elucidated below) the wavefunction of the $S_1$ state collapses to a pure CT, so that SS-CASPT2 and MS-CASPT2 give similar results. Furthermore, Figure S6 and Table S1 demonstrate that there exist a linear relation between the CASSCF and SS-CASPT2 potential energy surface profiles (at least along the minimum energy path) in all three systems, in line with previous works on Rh[2, 21]. As elaborated previously, the proportionality in the energies translates in proportionality in the resulting energy gradients and, finally, in a scaling factor to the simulation time[2, 21] but it should not affect the qualitative outcome of the comparison. Moreover, as foreshadowed in the previous section and elaborated below, the remarkable differences in the photoreactivity of the three pigments are to be also traced back to the mechanical tension in the catalytic cavity, which CASSCF is able to reproduce.

**Table S4**. SS–CASPT2 and MS–CASPT2//CASSCF(12,12)/6–31G*/AMBER calculation of averaged absorption maxima ($\lambda_{max}$, nm), vertical excitation energies $\Delta E$ (kcal/mol), oscillator strengths f, state–averaged using three roots (weights: 1/3, 1/3, 1/3) over all the 60 starting geometries of each pigment ensemble.

| | **SS–CASPT2** | | | | | | **MS–CASPT2** | | | | | |
|---|---|---|---|---|---|---|---|---|---|---|---|---|
| **Model** | $\lambda_1$ | $\lambda_2$ | $\Delta E_1$ | $\Delta E_2$ | $f_1$ | $f_2$ | $\lambda_1$ | $\lambda_2$ | $\Delta E_1$ | $\Delta E_2$ | $f_1$ | $f_2$ |
| **hMeOp** | 496 | 351 | 57.8 | 81.9 | 0.59 | 0.24 | 478 | 331 | 60.0 | 86.8 | 1.14 | 0.10 |
| **SqRh** | 488 | 354 | 58.9 | 81.7 | 0.49 | 0.31 | 481 | 328 | 59.8 | 87.6 | 1.04 | 0.13 |
| **Rh** | 497 | 355 | 57.9 | 81.6 | 0.48 | 0.34 | 488 | 321 | 59.0 | 89.5 | 1.17 | 0.12 |

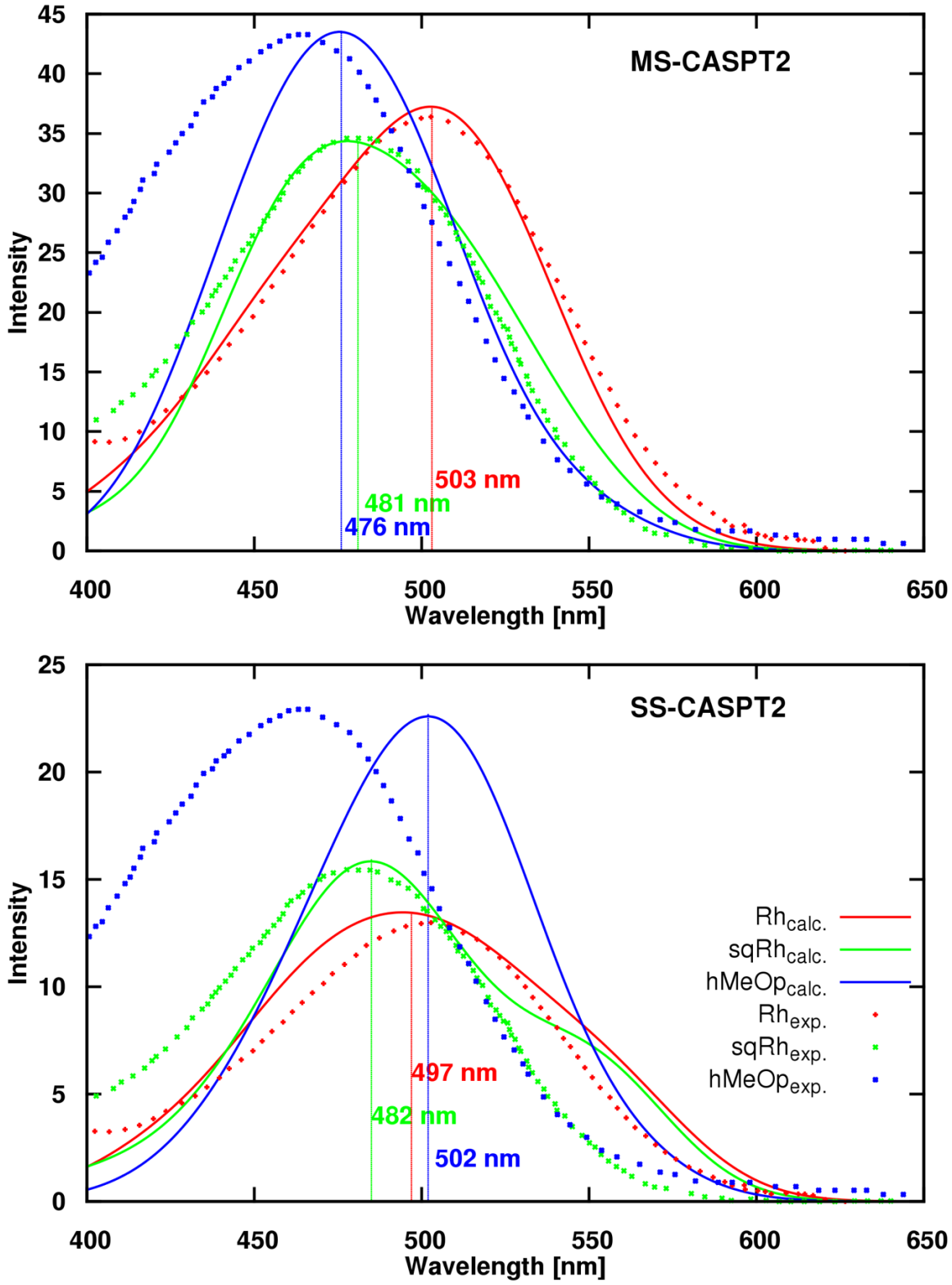


**Figure S8**. Experimental (dashed lines) and simulated (solid lines) linear absorption spectra of the three rhodopsins. Simulated spectra obtained from averaging over 60 realizations per pigment and corrected using MS-CASPT2 (top-panel) and SS–CASPT2 (bottom-panel) after SA3–CASSCF (12,12) calculations. Convolution based on wavelength values and $S_1/S_2$ oscillator strengths, Gaussian FWHM=53 nm. Exp. data taken from refs [29], [30] and [35] for hMeOp, sqRh and Rh, respectively.

## 5 Relationship between Vertical Excitation Energy, Steric Strain and Isomerization Speed

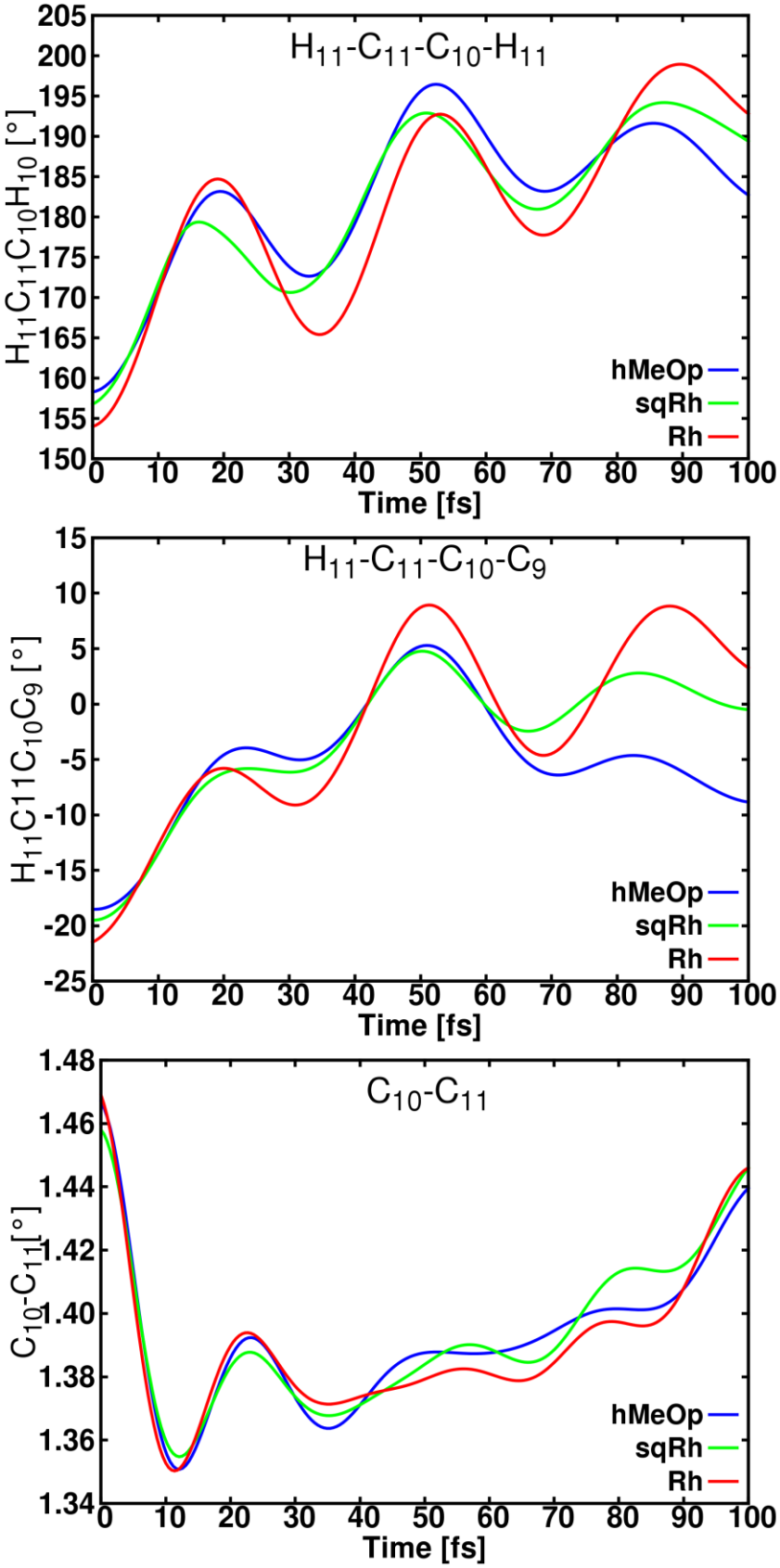


**Figure S9**. Characteristic geometrical parameters in the three pigments and their temporal evolution.

# 6 Rationalization of the Computed Quantum Yields

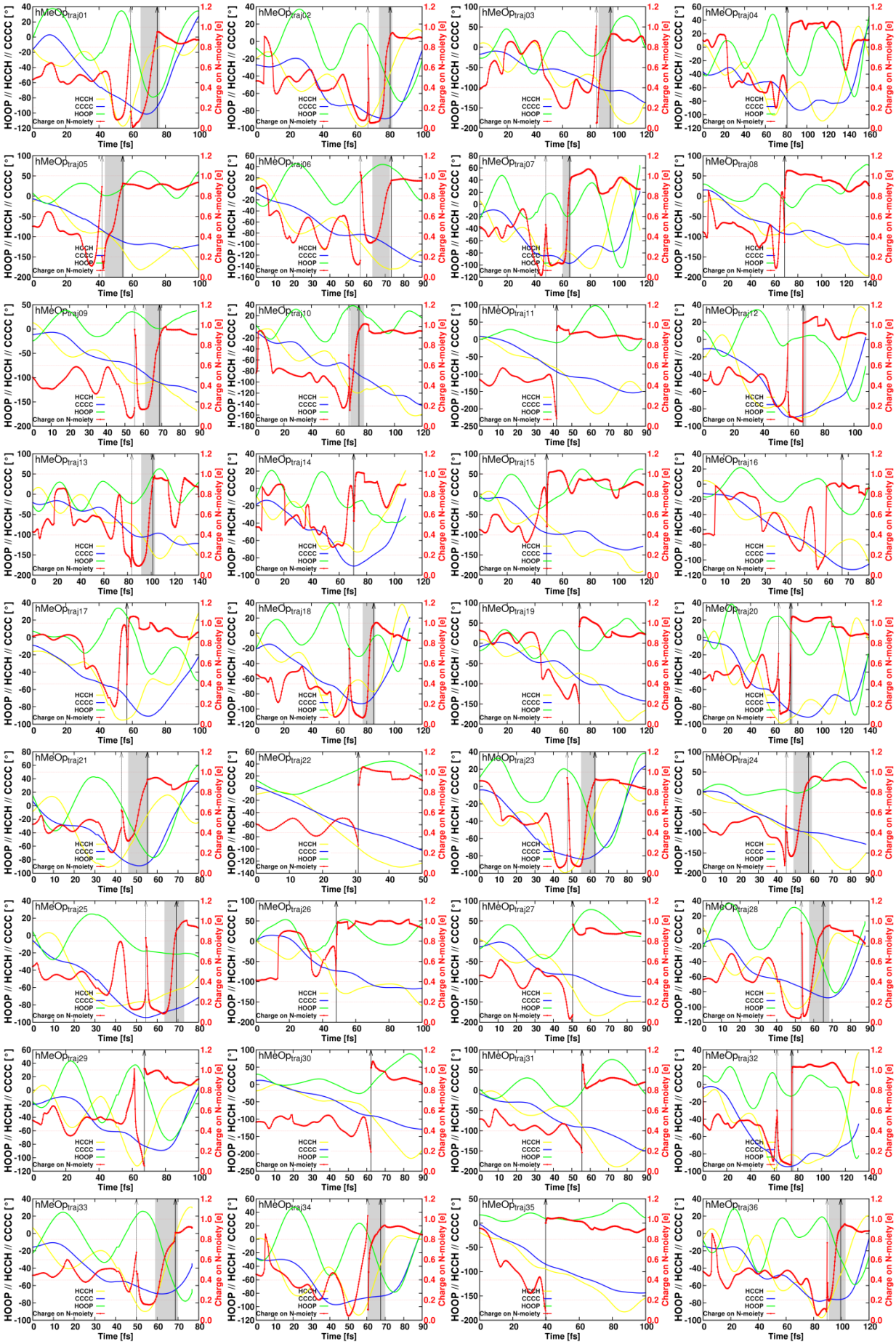

**continue Figure S10**

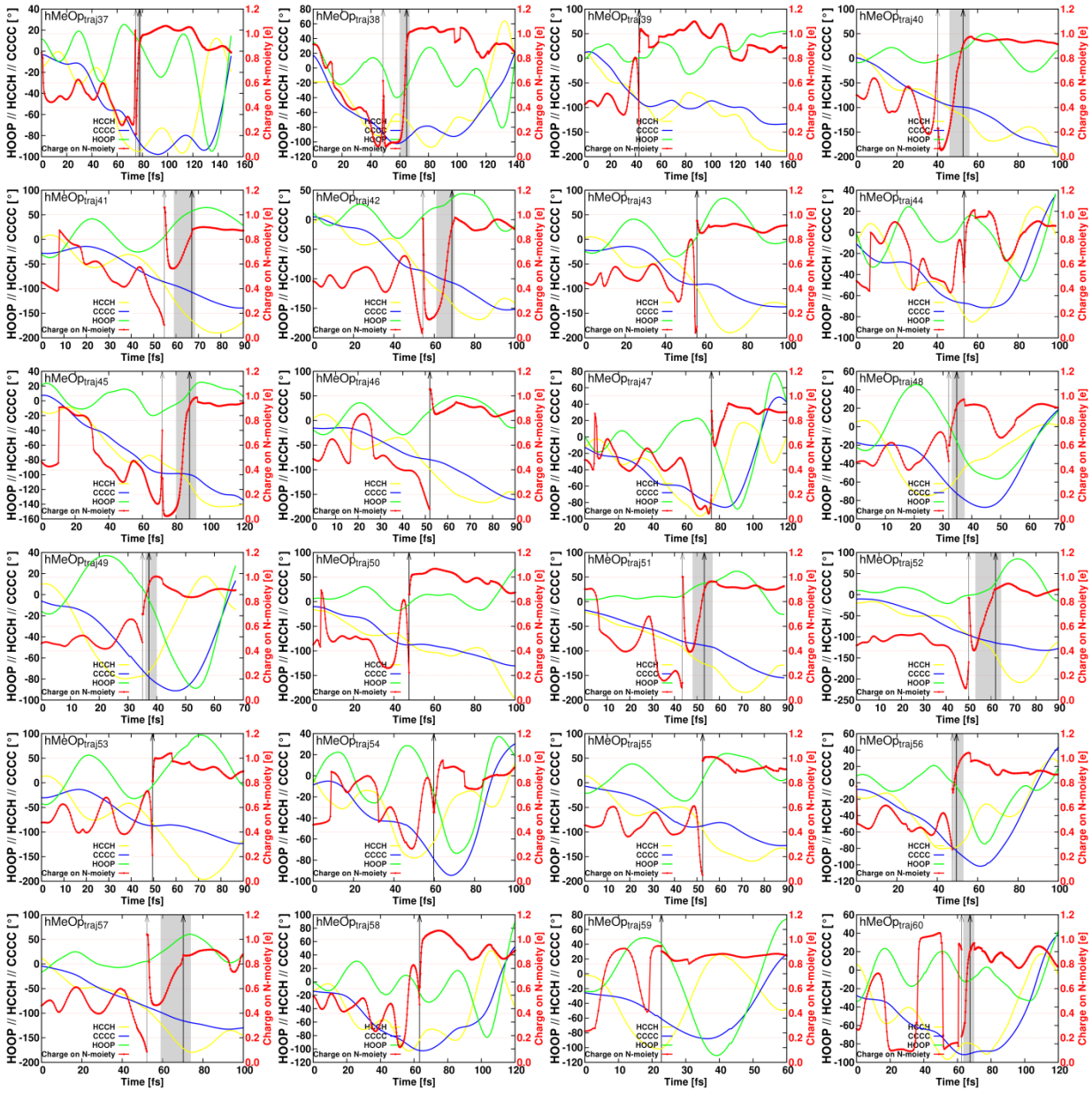


**Figure S10**. Evolution of $C_{10}C_{11}C_{12}C_{13}$, $H_{11}C_{11}C_{12}H_{12}$, HOOP ($C_{10}C_{11}C_{12}C_{13}$ - $H_{11}C_{11}C_{12}H_{12}$) and charge on N-moiety($C_{12}$---N fragment) of each trajectory of hMeOp during the simulation time, gray-shaded areas denote the time span in which the WF changes from CT to covalent after a hopping event, vertical dashed and solid arrows show the hopping and decision times, respectively.

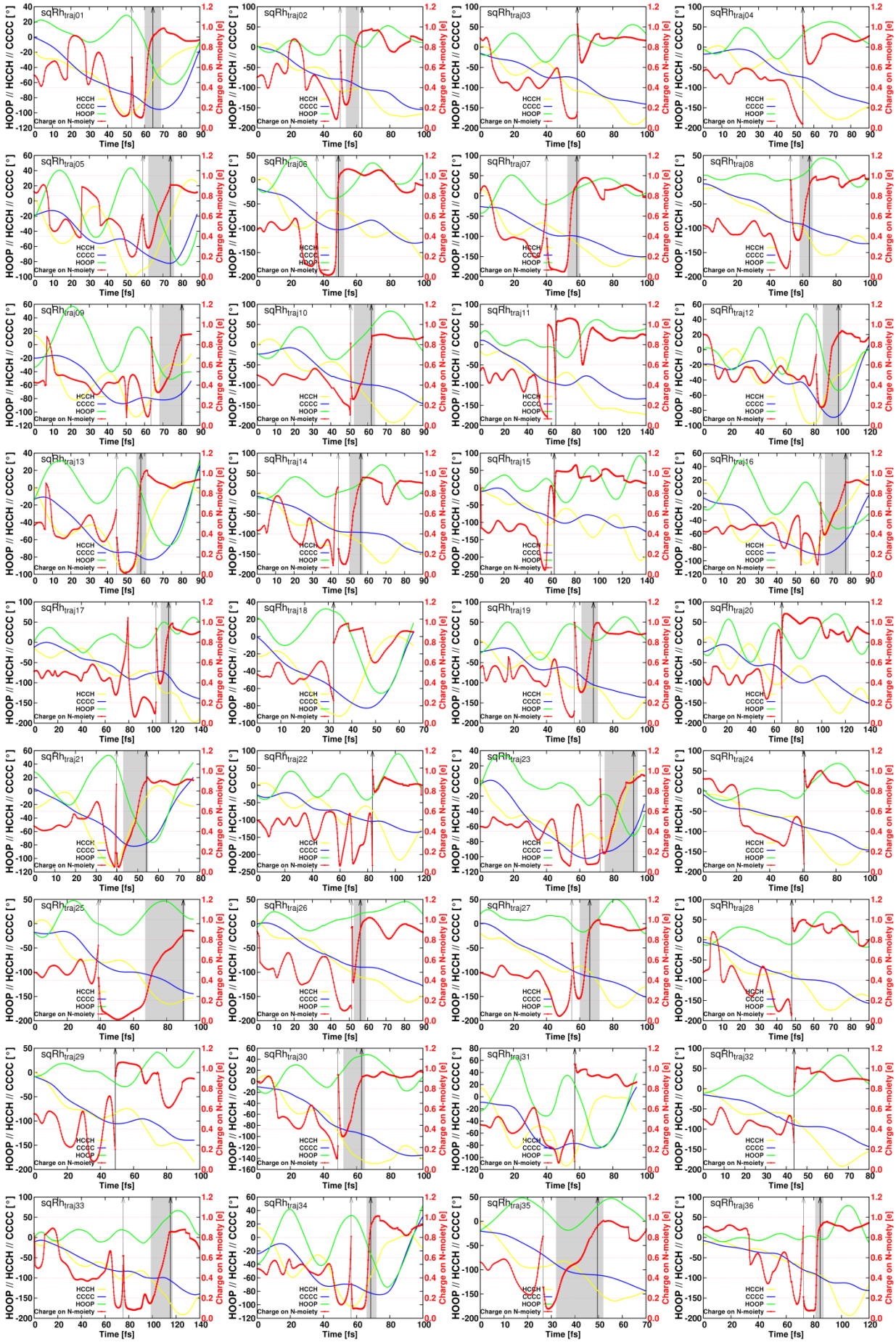
sqRh_traj01
sqRh_traj02
sqRh_traj03
sqRh_traj04
sqRh_traj05
sqRh_traj06
sqRh_traj07
sqRh_traj08
sqRh_traj09
sqRh_traj10
sqRh_traj11
sqRh_traj12
sqRh_traj13
sqRh_traj14
sqRh_traj15
sqRh_traj16
sqRh_traj17
sqRh_traj18
sqRh_traj19
sqRh_traj20
sqRh_traj21
sqRh_traj22
sqRh_traj23
sqRh_traj24
sqRh_traj25
sqRh_traj26
sqRh_traj27
sqRh_traj28
sqRh_traj29
sqRh_traj30
sqRh_traj31
sqRh_traj32
sqRh_traj33
sqRh_traj34
sqRh_traj35
sqRh_traj36
HOOP // HCCH // CCCC [°]
Charge on N-moiety [e]
Time [fs]
HCCH
CCCC
HOOP
Charge on N-moiety

**continue Figure S11**

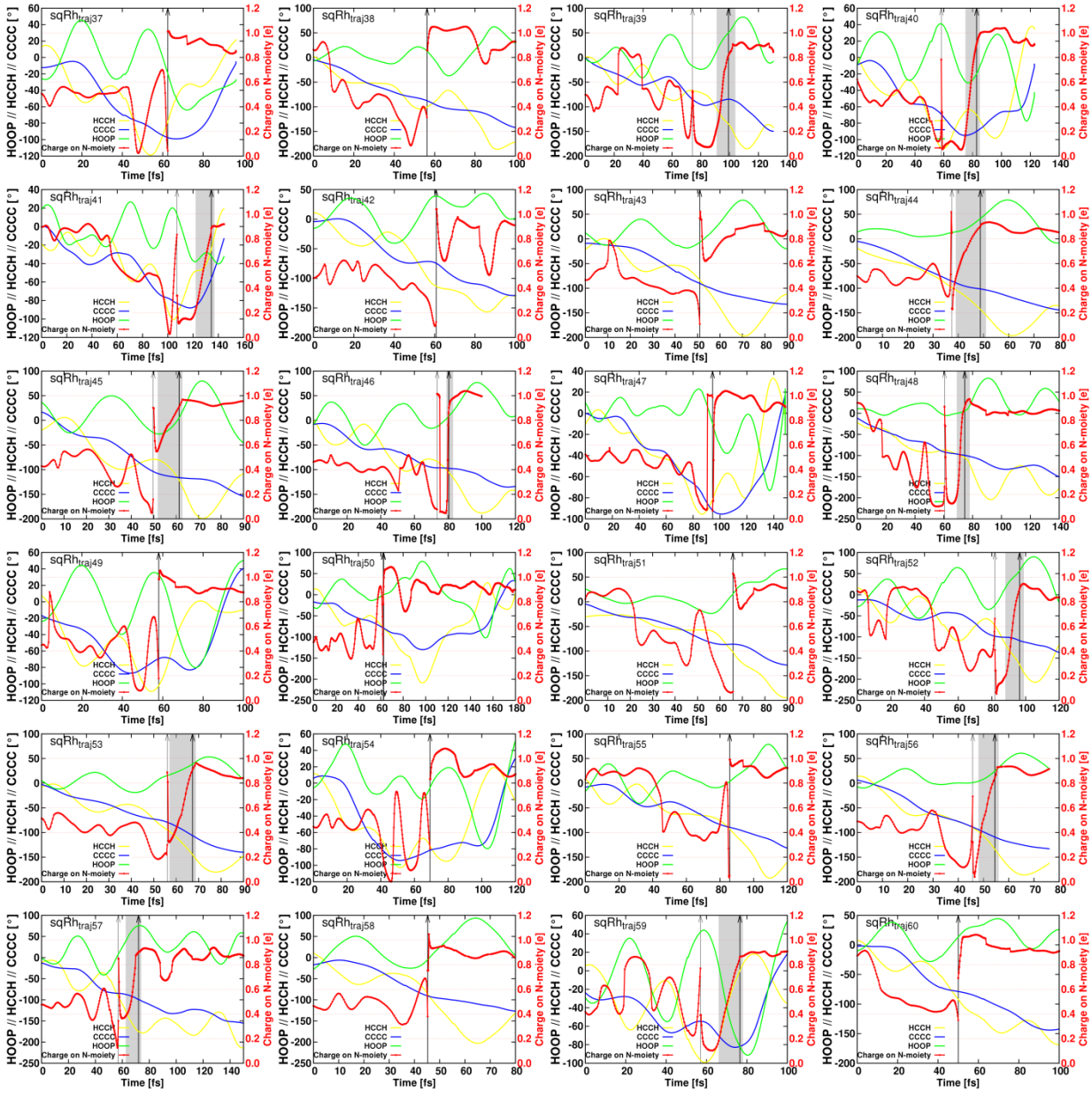


**Figure S11.** Evolution of $C_{10}C_{11}C_{12}C_{13}$, $H_{11}C_{11}C_{12}H_{12}$, HOOP and charge on N-moiety of each trajectory of sqRh during the simulation time, gray-shaded areas denote the time span in which the WF changes from CT to covalent after a hopping event, vertical dashed and solid arrows show the hopping and decision times, respectively.

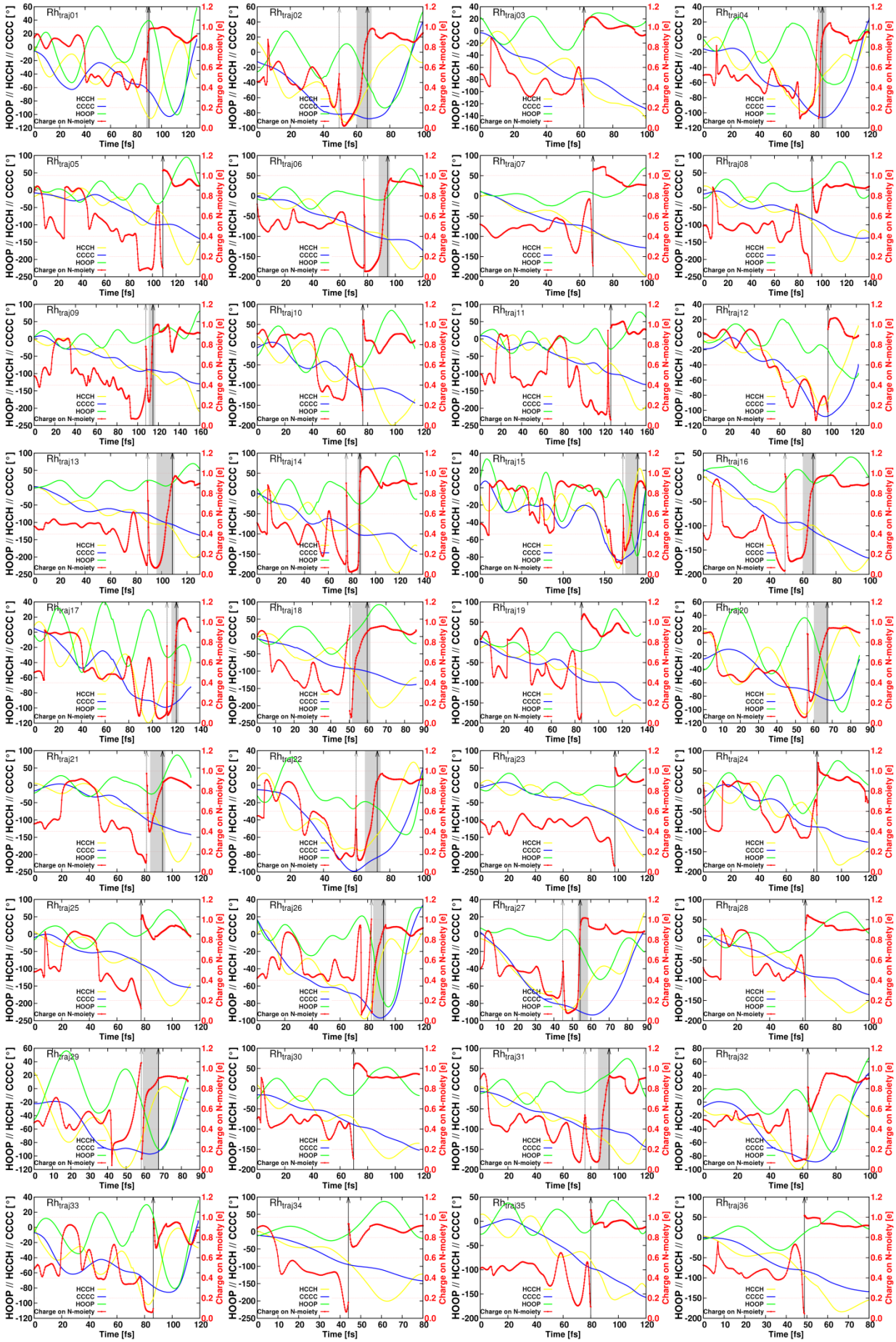
Rhtraj01
Rhtraj02
Rhtraj03
Rhtraj04
Rhtraj05
Rhtraj06
Rhtraj07
Rhtraj08
Rhtraj09
Rhtraj10
Rhtraj11
Rhtraj12
Rhtraj13
Rhtraj14
Rhtraj15
Rhtraj16
Rhtraj17
Rhtraj18
Rhtraj19
Rhtraj20
Rhtraj21
Rhtraj22
Rhtraj23
Rhtraj24
Rhtraj25
Rhtraj26
Rhtraj27
Rhtraj28
Rhtraj29
Rhtraj30
Rhtraj31
Rhtraj32
Rhtraj33
Rhtraj34
Rhtraj35
Rhtraj36
HOOP // HCCH // CCCC [ ° ]
Charge on N-moiety [e]
Time [fs]
HCCH
CCCC
HOOP
Charge on N-moiety

**continue Figure S12**

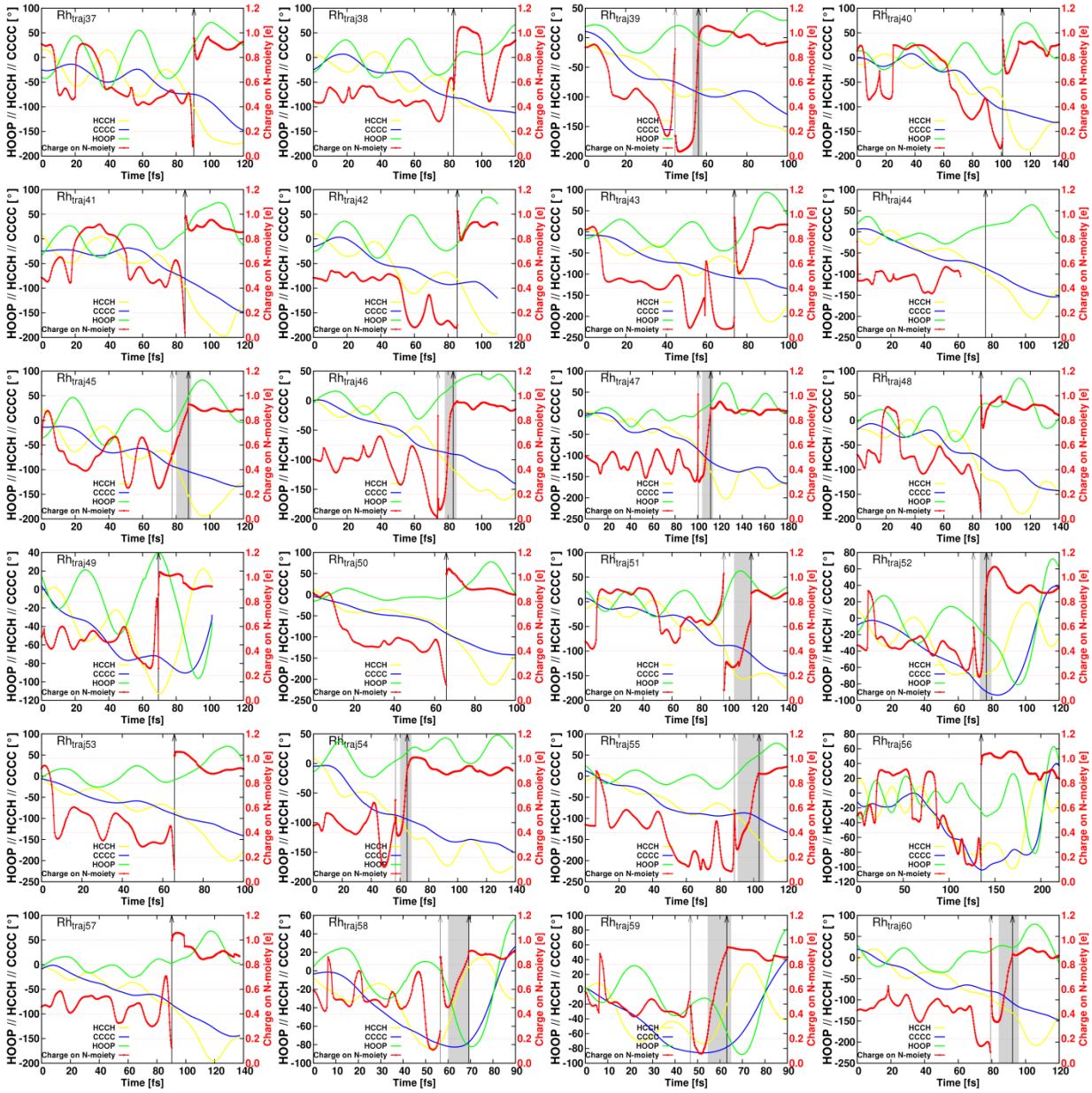


**Figure S12.** Evolution of $C_{10}C_{11}C_{12}C_{13}$, $H_{11}C_{11}C_{12}H_{12}$, HOOP and charge on N-moiety for each trajectory of Rh during the simulation time, gray-shaded areas denote the time span in which the WF changes from CT to covalent after a hopping event, vertical dashed and solid arrows show the hopping and decision times, respectively.

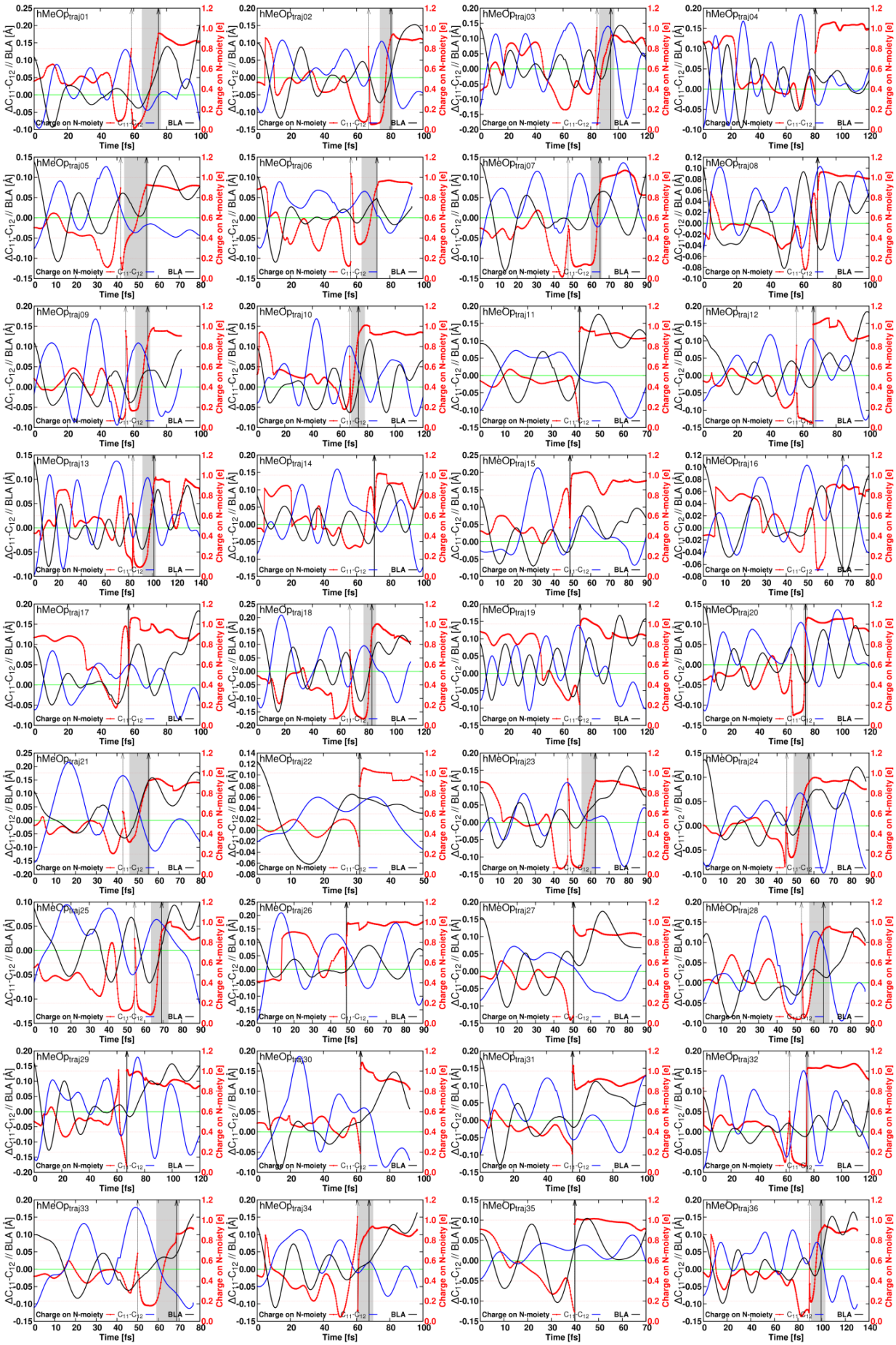
hMeOptraj01
hMeOptraj02
hMeOptraj03
hMeOptraj04
hMeOptraj05
hMeOptraj06
hMeOptraj07
hMeOptraj08
hMeOptraj09
hMeOptraj10
hMeOptraj11
hMeOptraj12
hMeOptraj13
hMeOptraj14
hMeOptraj15
hMeOptraj16
hMeOptraj17
hMeOptraj18
hMeOptraj19
hMeOptraj20
hMeOptraj21
hMeOptraj22
hMeOptraj23
hMeOptraj24
hMeOptraj25
hMeOptraj26
hMeOptraj27
hMeOptraj28
hMeOptraj29
hMeOptraj30
hMeOptraj31
hMeOptraj32
hMeOptraj33
hMeOptraj34
hMeOptraj35
hMeOptraj36
ΔC11-C12 // BLA [Å]
Charge on N-moiety [e]
Time [fs]
Charge on N-moiety
C11-C12
BLA

**continue Figure S13**

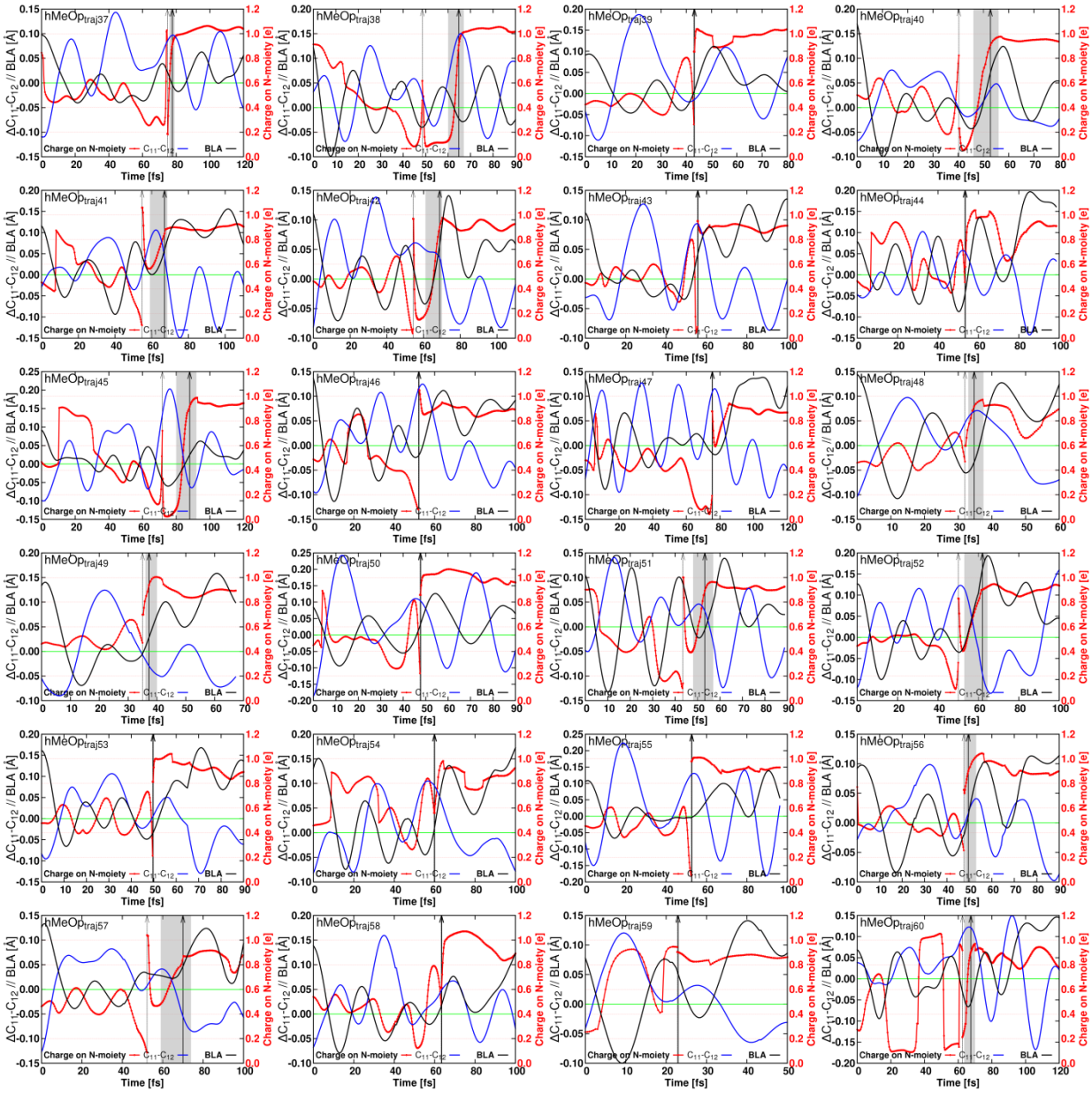


**Figure S13**. Evolution of BLA, $C_{11}C_{12}$ and charge on N-moiety for each trajectory of hMeOp during the simulation time ($\Delta C_{11}$-$C_{12}$ represents the deviation of $C_{11}$-$C_{12}$ form 1.45Å), gray-shaded areas denote the time span in which the WF changes from CT to covalent after a hopping event, vertical dashed and solid arrows show the hopping and decision times, respectively.

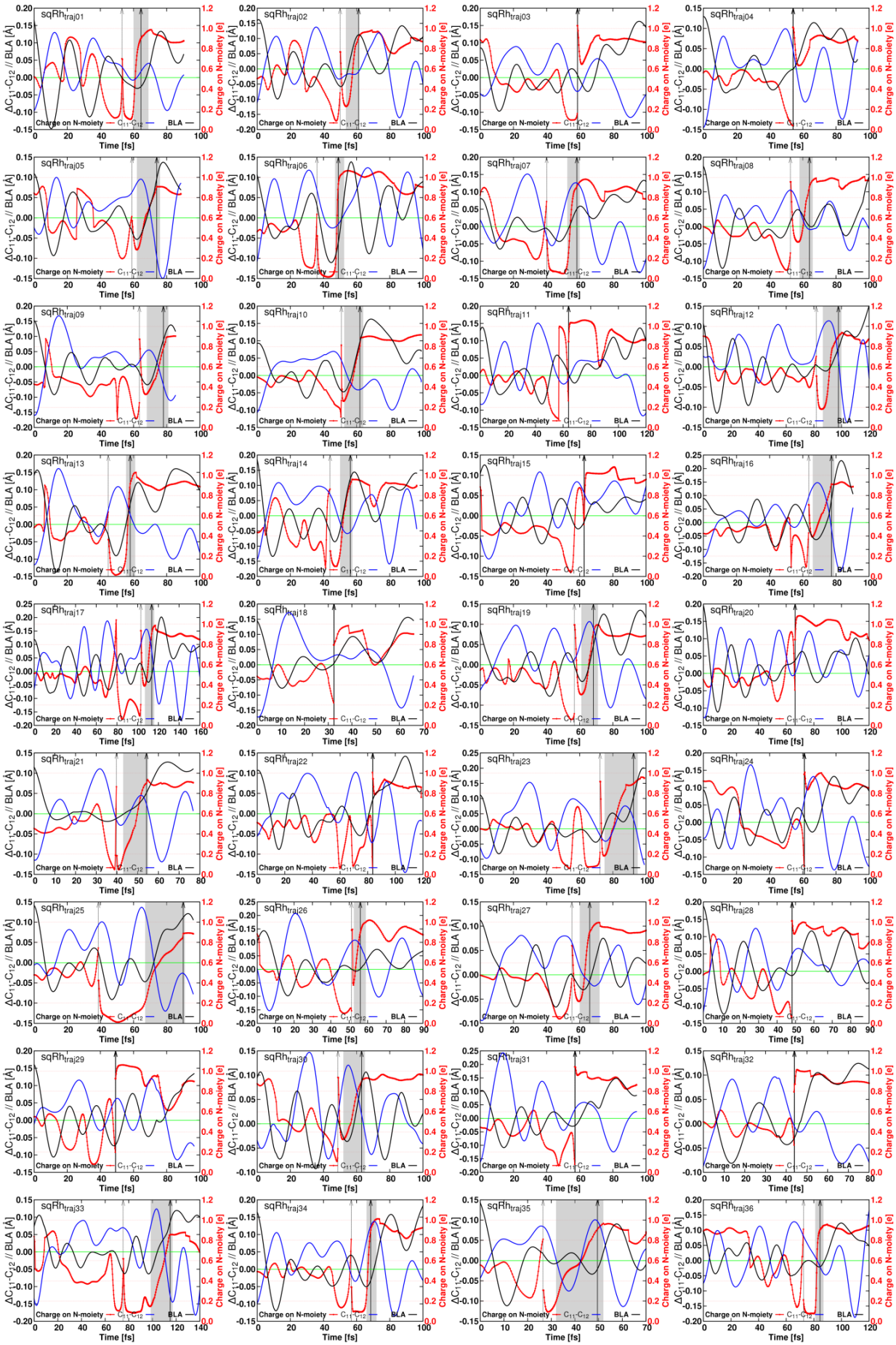
sqRh traj01
sqRh traj02
sqRh traj03
sqRh traj04
sqRh traj05
sqRh traj06
sqRh traj07
sqRh traj08
sqRh traj09
sqRh traj10
sqRh traj11
sqRh traj12
sqRh traj13
sqRh traj14
sqRh traj15
sqRh traj16
sqRh traj17
sqRh traj18
sqRh traj19
sqRh traj20
sqRh traj21
sqRh traj22
sqRh traj23
sqRh traj24
sqRh traj25
sqRh traj26
sqRh traj27
sqRh traj28
sqRh traj29
sqRh traj30
sqRh traj31
sqRh traj32
sqRh traj33
sqRh traj34
sqRh traj35
sqRh traj36
ΔC11-C12 // BLA [Å]
Charge on N-moiety [e]
Time [fs]
Charge on N-moiety
C11-C12
BLA

**continue Figure S14**

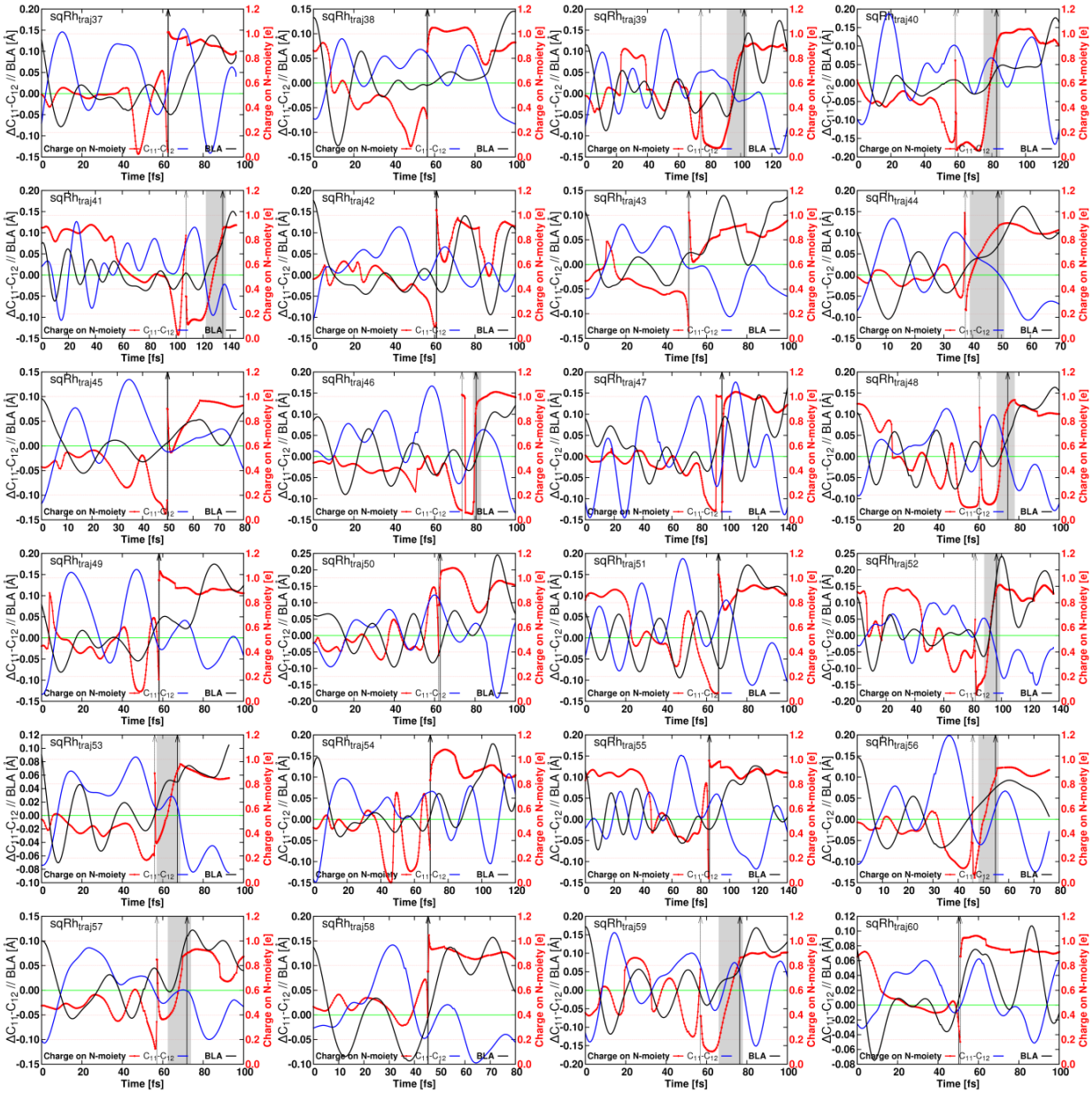


**Figure S14.** Evolution of BLA, $C_{11}C_{12}$ and charge on N-moiety for each trajectory of sqRh during the simulation time ($\Delta C_{11}$-$C_{12}$ represents the deviation of $C_{11}$-$C_{12}$ form 1.45Å), gray-shaded areas denote the time span in which the WF changes from CT to covalent after a hopping event, vertical dashed and solid arrows show the hopping and decision times, respectively.

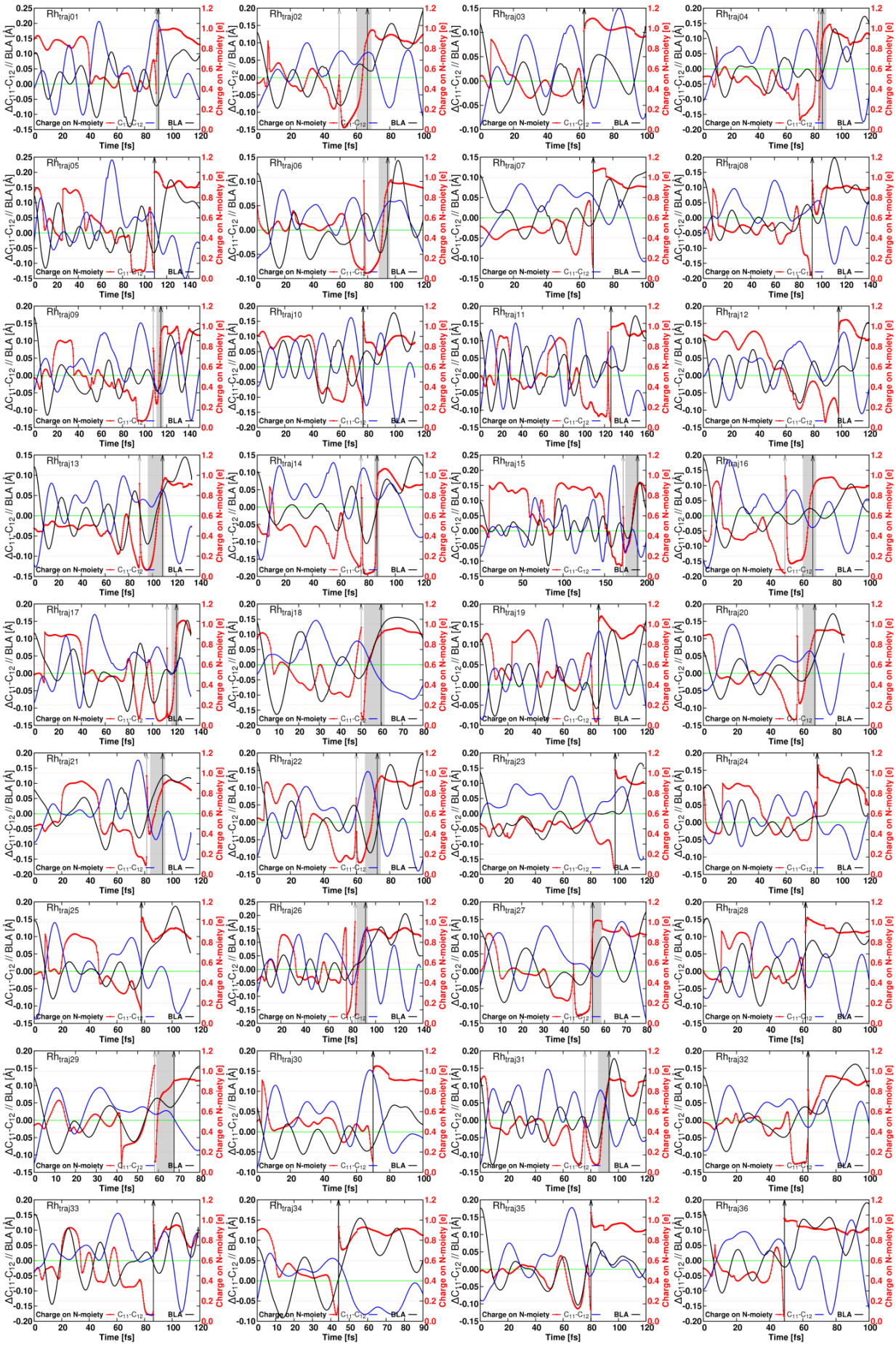
Rh traj01
Rh traj02
Rh traj03
Rh traj04
Rh traj05
Rh traj06
Rh traj07
Rh traj08
Rh traj09
Rh traj10
Rh traj11
Rh traj12
Rh traj13
Rh traj14
Rh traj15
Rh traj16
Rh traj17
Rh traj18
Rh traj19
Rh traj20
Rh traj21
Rh traj22
Rh traj23
Rh traj24
Rh traj25
Rh traj26
Rh traj27
Rh traj28
Rh traj29
Rh traj30
Rh traj31
Rh traj32
Rh traj33
Rh traj34
Rh traj35
Rh traj36
ΔC11-C12 // BLA [Å]
Charge on N-moiety [e]
Time [fs]
Charge on N-moiety
C11-C12
BLA

**continue Figure S15**

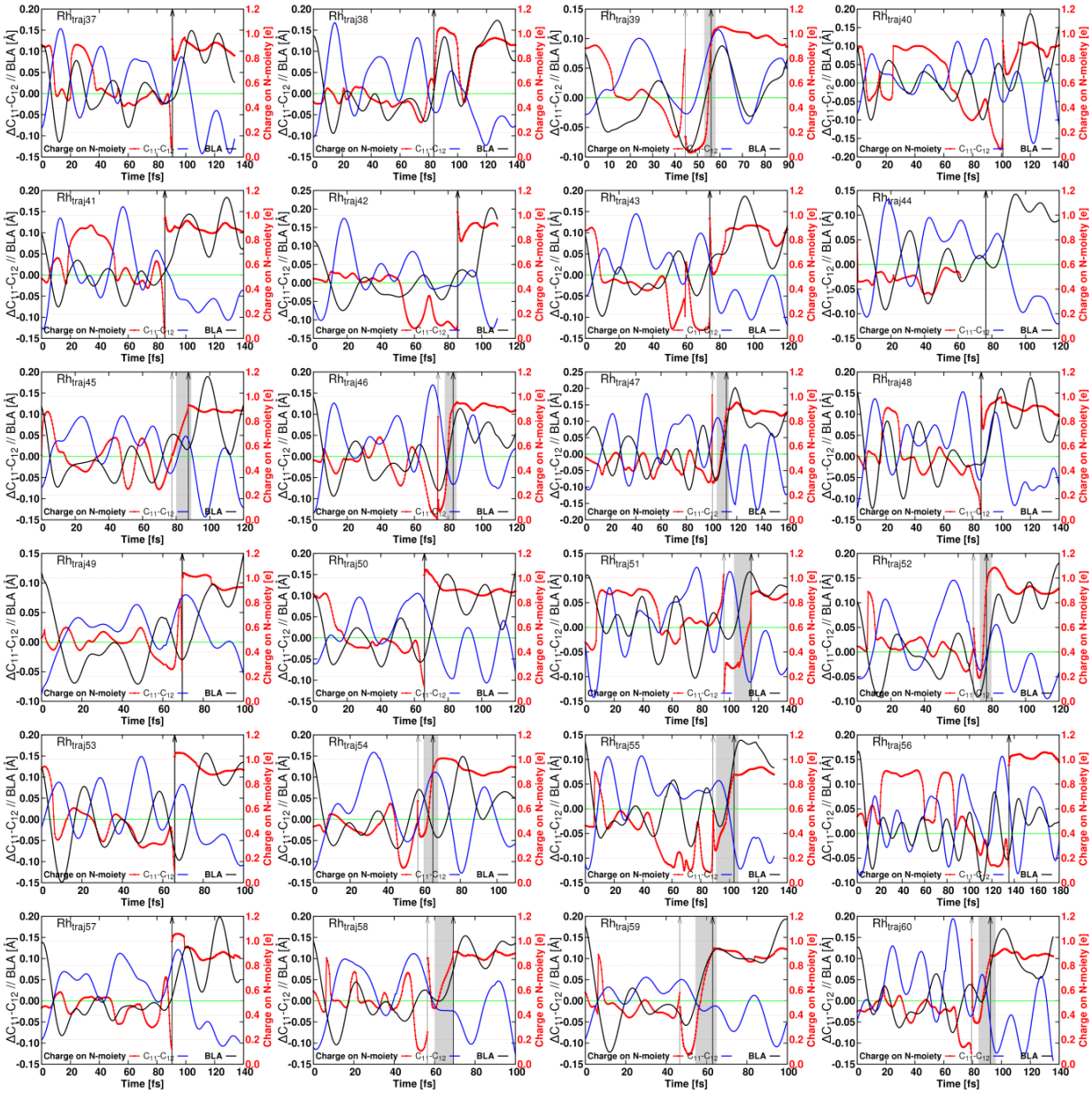


**Figure S15**. Evolution of BLA, $C_{11}C_{12}$ and charge on N-moiety for each trajectory of Rh during the simulation time ($\Delta C_{11}$-$C_{12}$ represents the deviation of $C_{11}$-$C_{12}$ form 1.45Å), gray-shaded areas denote the time span in which the WF changes from CT to covalent after a hopping event, vertical dashed and solid arrows show the hopping and decision times, respectively.

## 7 Conclusion remarks

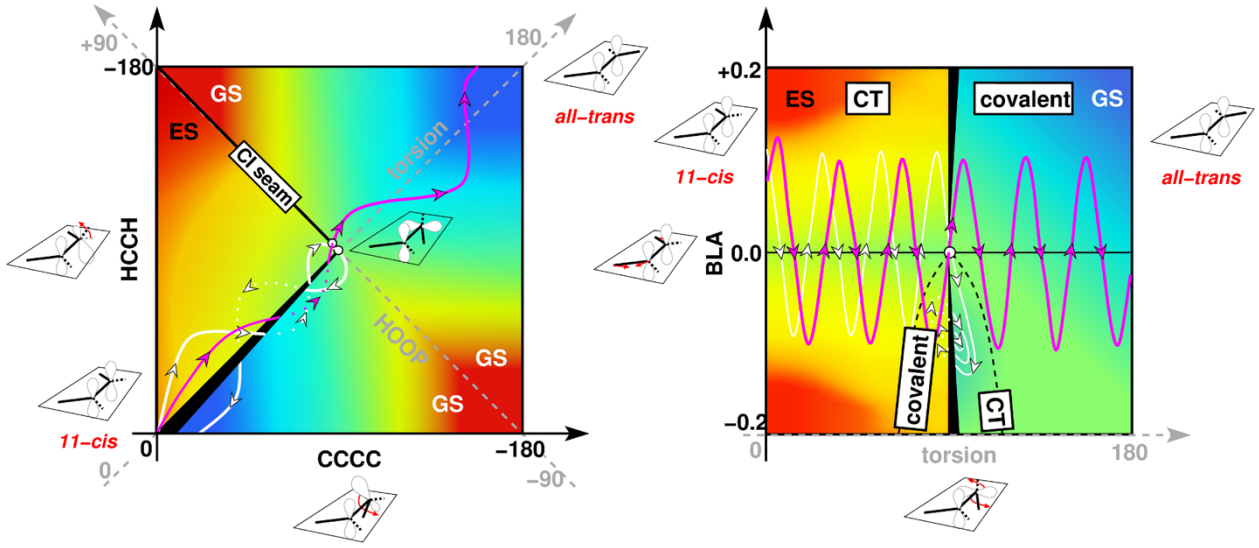


**Figure S16.** Schematic maps of the *two-states* / *three-modes* model characterizing the 11-*cis*->all-*trans* isomerization of animal rhodopsins. Color gradient represents PES topography, where red depicts the highest and blue the lowest energy regions. **Left**: Scheme of the reaction in the subspace of CCCC and HCCH, both running in counter-clockwise direction from 0° to -180°. The diagonals define the collective coordinates "torsion" (0.5*CCCC+0.5*HCCH, defined from 0° to +180°) and hydrogen-out-of-plane (HOOP, 0.5*CCCC-0.5*HCCH, defined from -90° to +90°). The triangular area delimited by torsion [0°:90°] and HOOP [0°:90°] shows the ES PES, the remaining area shows the GS PES. ES/GS degeneracy (i.e. CI seam) is preserved along the HOOP coordinate for a 90° torsion. The CI seam (solid black line) is shown only for positive values of the HOOP angle [0°:90°]. **Right**: Scheme of the reaction in the subspace of torsion (more precisely, any collective CCCC+HCCH motion that drives the system towards the CI seam) and bond length alternation (BLA). The area delimited by torsion [0°:90°] shows the ES PES, the area delimited by torsion [90°:180°] shows the GS PES. ES and GS intersect in the center of the graph (i.e. CI). In each graph two trajectories are drawn, a reactive one that reaches all-trans (magenta full/dotted curves) and a non-reactive one which returns back to 11-cis (white full/dotted curves). Dots highlight that the evolution proceeds in a region of the PES not visible in the graphs. The evolution depends on the relative phases of the three coordinates at "hopping event" (i.e. decay through the CI seam, “hopping " point denoted by a circle in Figure S16) and at "decision event".

**Table S5.** Classification the trajectories according to correlation between the BLA and the switching of the electronic structure toward covalent state.

| | | **Rh** | **sqRh** | **hMeOp** |
|---|---|---|---|---|
| **hop occurs with covalent characters (i.e. decision is taken at hop)** | the WF adopts covalent character upon hop to the GS, thus, hop and decision time coincide; BLA is not decisive in these cases | 3, 5, 7, 8, 10, 11, 12, 19, 23, 24, 25, 28, 30, 32, 33, 34, 35, 36, 37, 38, 40, 41, 42, 43, 44, 48, 49, 50, 53, 56, 57 | 3, 4, 11, 15, 18, 20, 22, 24, 28, 29, 31, 32, 37, 38, 42, 43, 47, 49, 50, 51, 54, 55, 58, 60 | 4, 8, 11, 14, 15, 16, 17, 19, 22, 26, 27, 29, 30, 31, 35, 39, 43, 44, 46, 47, 50, 53, 54, 55, 58, 59 |
| | **number of trajectories** | **31** | **24** | **26** |
| **the switching to biradical WF occurs after hopping time (i.e. at the decision time)** | BLA increases while $C_{11}$-$C_{12}$ decreases when the GS WF character changes from CT to covalent | 1, 4, 9, 14, 15, 18, 20, 21, 22, 27, 31, 46, 47, 51, 55, 58, 59, 60 | 5, 9, 10, 12, 13, 14, 16, 17, 19, 23, 26, 27, 30, 33, 39, 44, 48, 52 | 2, 3, 6, 7, 9, 10, 12, 13, 18, 21, 24, 25, 32, 33, 41, 42, 45, 49, 51, 52, 57, 60 |
| | **number of trajectories** | **18** | **18** | **22** |
| | both BLA and $C_{11}$-$C_{12}$ increases when the GS WF character changes from CT to covalent | 6, 13, 17, 26, 39, 52 | 1, 2, 6, 7, 21, 25, 34, 40, 41, 45, 46, 53, 56, 57, 59 | 1, 5, 23, 34, 36, 40, 48, 56 |
| | **number of trajectories** | **6** | **15** | **8** |
| | Both BLA and $C_{11}$-$C_{12}$ decrease when the GS WF character changes from CT to covalent (outliers) | 2, 16, 29, 45, 54 | 8, 35, 36 | 20, 28, 37, 38 |
| | **number of trajectories** | **5** | **3** | **4** |

## 8 Statistical Results

The distribution of $S_1/S_0$ energy gaps at the decay points shows that a non-negligible percentage of the ensemble decays while the $S_1/S_0$ gap is relatively large. However, most of the trajectories decay to the ground state close to the crossing, and the number of decay events decreases with the increase of the $S_0/S_1$ energy gap (**Figure S17**). **Figure S18** depicts the distribution of hopping events as a function of the CCCC torsion value, exhibiting a typical Gaussian like shape centered around 80-90°. The average retinal coordinates over all ensemble members at the decay points are given in **Table S6**, showing similar properties for all pigments.

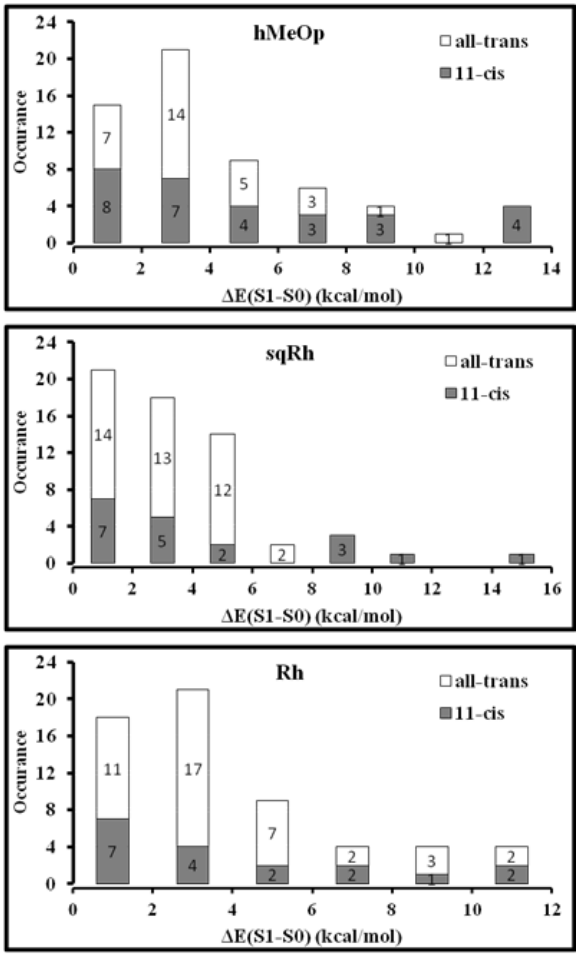


**Figure S17**. Distribution of hopping events as a function of the CASSCF energy differences $\Delta E(S_1\text{-}S_0)$ for hMeOp (top), sqRh (middle) and Rh (bottom). The height of the bar graphs corresponds to the number of trans (nofill) and cis (gray) photoproducts of individual trajectories.

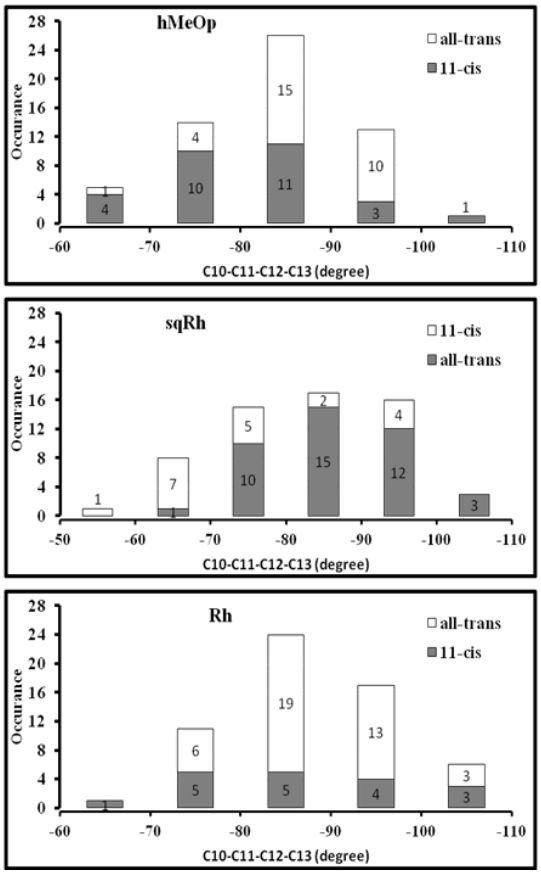


**Figure S18**. Distribution of hopping events as a function of the $C_{10}$–$C_{11}$–$C_{12}$–$C_{13}$ torsion for hMeOp (top), sqRh (middle) and Rh (bottom). The height of the bar graphs corresponds to the number of trans (nofill) and cis (gray) photoproducts of individual trajectories.

**Table S6**. Averaged retinal geometry parameters in the three pigments at the hopping point.

| Parameter | hMeOp | sqRh | Rh |
|---|---|---|---|
| $C_5$–$C_6$ | 1.339 | 1.333 | 1.345 |
| $C_6$–$C_7$ | 1.482 | 1.478 | 1.489 |
| $C_7$–$C_8$ | 1.380 | 1.375 | 1.373 |
| $C_8$–$C_9$ | 1.445 | 1.436 | 1.427 |
| $C_9$–$C_{10}$ | 1.421 | 1.438 | 1.450 |
| $C_{10}$–$C_{11}$ | 1.388 | 1.382 | 1.381 |
| $C_{11}$–$C_{12}$ | 1.492 | 1.481 | 1.482 |
| $C_{12}$–$C_{13}$ | 1.373 | 1.378 | 1.370 |
| $C_{13}$–$C_{14}$ | 1.453 | 1.468 | 1.466 |
| $C_{14}$–$C_{15}$ | 1.369 | 1.369 | 1.366 |
| $C_{15}$–N | 1.375 | 1.384 | 1.365 |
| $C_8$–$C_9$–$C_{10}$–$C_{11}$ | 143.3 | 143.3 | 149.1 |
| $C_{10}$–$C_{11}$–$C_{12}$–$C_{13}$ | 84.0 | 83.4 | 88.1 |
| $C_{12}$–$C_{13}$–$C_{14}$–$C_{15}$ | 167.7 | 165.4 | 166.3 |
| $C_8$–$C_9$–$C_{10}$–H | 23.7 | 25.2 | 24.3 |
| H–$C_{11}$–$C_{12}$–$C_{13}$ | 90.1 | 89.7 | 87.6 |
| $C_{10}$–$C_{11}$–$C_{12}$–H | 97.6 | 96.6 | 99.6 |
| $C_{12}$–$C_{13}$–$C_{17}$–H | 15.4 | 15.7 | 14.7 |
| H–$C_{15}$–N–H | 165.5 | 165.4 | 167.1 |
| H–$C_{11}$–$C_{12}$–H | 88.3 | 90.2 | 84.8 |

**Table S7***. Statistical analysis of the individual trajectories of the hMeOp ensemble showing the hopping /decision times, the direction of the $HC_{11}C_{12}H$, HOOP, $CC_{11}C_{12}C$ and the leading modes, and the computed and expected photoproduct distributions at both hopping/decision times.

| Traj | hopping time (fs) | Product formation follows … | | | leading mode | decision time (fs) | Product formation follows … | | | leading mode | Computed Product | | Expected Product at hopping time | | Expected Product at decision time | |
|---|---|---|---|---|---|---|---|---|---|---|---|---|---|---|---|---|
| | | $HC_{11}$-$C_{12}H$ at hopping time | HOOP at hopping time | $CC_{11}C_{12}C$ at hopping time | | | $HC_{11}C_{12}H$ at decision time | HOOP at decision time | $CC_{11}C_{12}C$ at decision time | | Trans | Cis | Trans | Cis | Trans | Cis |
| **01** | 58.75 | T | T | F | HCCH | 75.00 | T | F | T | CCCC | | √ | | √ | | √ |
| **02** | 67.25 | T | T | F | HCCH | 80.75 | T | T | T | HCCH | | √ | | √ | | √ |
| **03** | 84.50 | T | T | T | HCCH | 94.50 | T | T | T | HCCH | √ | | √ | | √ | |
| **04** | 81.00 | T | T | T | N/A | 81.00 | T | T | F | N/A | | √ | | √ | | √ |
| **05** | 41.75 | T | F | T | CCCC | 54.25 | T | T | T | HCCH | √ | | √ | | √ | |
| **06** | 56.50 | T | T | T | HCCH | 72.25 | N/A | F | T | CCCC | √ | | √ | | - | |
| **07** | 47.75 | F | F | N/A | HCCH | 65.00 | F | T | N/A | N/A | | √ | √ | | √ | |
| **08** | 68.75 | F | F | T | N/A | 68.75 | F | F | T | N/A | √ | | | √ | | √ |
| **09** | 55.25 | T | N/A | T | CCCC | 68.50 | T | N/A | T | HCCH | √ | | √ | | √ | |
| **10** | 67.00 | T | N/A | T | CCCC | 73.25 | F | F | T | CCCC | √ | | √ | | | √ |
| **11** | 41.75 | T | T | T | HCCH/CCCC | 41.75 | T | T | T | HCCH | √ | | √ | | √ | |
| **12** | 57.00 | F | F | N/A | N/A | 66.25 | T | F | T | CCCC | | √ | √ | | | √ |
| **13** | 83.50 | T | N/A | T | HCCH | 101.25 | T | T | F | HCCH | √ | | √ | | √ | |
| **14** | 70.50 | F | F | T | CCCC | 70.50 | N/A | F | T | CCCC | | √ | √ | | - | |
| **15** | 48.50 | T | T | T | HCCH | 48.50 | T | T | T | HCCH | √ | | √ | | √ | |
| **16** | 67.00 | F | F | T | CCCC | 67.00 | F | F | T | CCCC | √ | | | √ | | √ |
| **17** | 56.75 | T | T | F | HCCH | 56.75 | T | T | F | HCCH | | √ | | √ | | √ |
| **18** | 67.00 | T | T | F | CCCC | 83.00 | F | F | T | CCCC | | √ | | √ | √ | |
| **19** | 72.00 | T | F | T | CCCC | 72.00 | T | F | T | CCCC | √ | | √ | | √ | |
| **20** | 63.75 | F | N/A | F | CCCC | 74.00 | T | T | F | HCCH | | √ | √ | | | √ |
| **21** | 42.75 | T | T | F | HCCH | 55.25 | T | T | T | HCCH | | √ | | √ | | √ |
| **22** | 30.75 | T | T | T | HCCH | 30.75 | T | T | T | HCCH | √ | | √ | | √ | |
| **23** | 47.50 | T | T | T | HCCH | 62.50 | T | T | T | HCCH | | √ | | √ | | √ |
| **24** | 45.25 | T | F | T | CCCC | 57.25 | T | T | T | HCCH | √ | | √ | | √ | |
| **25** | 54.50 | T | T | T | HCCH | 69.25 | T | N/A | T | HCCH/CCCC | | √ | | √ | | √ |
| **26** | 48.25 | T | T | T | HCCH | 48.25 | T | T | T | HCCH | √ | | √ | | √ | |
| **27** | 50.50 | T | T | T | HCCH | 50.50 | T | T | T | HCCH | √ | | √ | | √ | |
| **28** | 53.25 | T | T | F | HCCH | 65.25 | T | T | N/A | HCCH | | √ | | √ | | √ |
| **29** | 67.00 | T | T | F | HCCH | 67.00 | T | T | F | HCCH | | √ | | √ | | √ |
| **30** | 62.25 | T | T | T | HCCH | 62.25 | T | T | T | HCCH | √ | | √ | | √ | |
| **31** | 55.50 | T | T | N/A | HCCH | 55.50 | T | T | N/A | HCCH | √ | | √ | | √ | |
| **32** | 62.00 | T | T | F | CCCC | 75.00 | F | F | T | N/A | | √ | | √ | √ | |
| **33** | 50.00 | F | F | F | N/A | 68.75 | T | T | T | HCCH | | √ | √ | | | √ |
| **34** | 60.50 | T | T | T | HCCH | 67.50 | T | T | T | HCCH | | √ | | √ | | √ |
| **35** | 39.75 | T | N/A | T | HCCH/CCCC | 39.75 | T | N/A | T | HCCH/CCCC | √ | | √ | | √ | |
| **36** | 89.75 | T | F | N/A | HCCH | 99.50 | T | T | T | HCCH | | √ | | √ | | √ |

**Continue Table S7**

| Traj | hopping time (fs) | Product formation follows … | | | leading mode | decision time (fs) | Product formation follows … | | | leading mode | Computed Product | | Expected Product at hopping time | | Expected Product at decision time | |
|---|---|---|---|---|---|---|---|---|---|---|---|---|---|---|---|---|
| | | $HC_{11}$-$C_{12}H$ at hopping time | HOOP at hopping time | $CC_{11}C_{12}C$ at hopping time | | | $HC_{11}C_{12}H$ at decision time | HOOP at decision time | $CC_{11}C_{12}C$ at decision time | | Trans | Cis | Trans | Cis | Trans | Cis |
| **37** | 74.75 | F | T | F | N/A | 77.75 | T | T | F | N/A | | √ | √ | | | √ |
| **38** | 48.50 | T | F | T | N/A | 64.75 | F | F | T | N/A | | √ | | √ | √ | |
| **39** | 43.00 | T | N/A | T | HCCH | 43.00 | T | T | T | N/A | √ | | √ | | √ | |
| **40** | 40.25 | T | T | T | HCCH | 52.75 | T | T | T | HCCH | √ | | √ | | √ | |
| **41** | 54.75 | T | T | T | HCCH | 67.00 | T | T | T | HCCH | √ | | √ | | √ | |
| **42** | 54.25 | T | T | T | CCCC | 68.75 | T | T | T | HCCH | √ | | √ | | √ | |
| **43** | 55.50 | T | T | N/A | HCCH | 55.50 | T | T | N/A | HCCH | √ | | √ | | √ | |
| **44** | 53.25 | F | T | F | HCCH | 53.25 | F | T | F | HCCH | | √ | √ | | - | |
| **45** | 71.75 | T | T | T | HCCH | 88.00 | T | T | T | HCCH | √ | | √ | | √ | |
| **46** | 52.00 | T | T | T | HCCH | 52.00 | T | T | T | HCCH | √ | | √ | | √ | |
| **47** | 75.25 | T | T | F | HCCH | 75.25 | T | T | F | HCCH | | √ | | √ | | √ |
| **48** | 32.00 | T | T | F | HCCH | 34.75 | T | T | F | HCCH | | √ | | √ | | √ |
| **49** | 35.00 | T | T | F | HCCH | 37.25 | T | T | F | HCCH | | √ | | √ | | √ |
| **50** | 47.50 | T | T | N/A | HCCH | 47.50 | T | T | N/A | HCCH | √ | | √ | | √ | |
| **51** | 43.50 | T | T | T | HCCH | 53.25 | T | T | T | HCCH | √ | | √ | | √ | |
| **52** | 50.00 | T | T | T | HCCH | 62.00 | T | T | T | HCCH | √ | | √ | | √ | |
| **53** | 49.50 | T | T | N/A | HCCH | 49.50 | T | T | N/A | HCCH | √ | | √ | | √ | |
| **54** | 59.75 | T | T | F | HCCH | 59.75 | T | T | F | HCCH | | √ | | √ | | √ |
| **55** | 52.50 | T | T | F | HCCH | 52.50 | T | T | F | HCCH | √ | | √ | | √ | |
| **56** | 47.50 | N/A | T | F | CCCC | 49.50 | T | T | F | HCCH | | √ | | | | √ |
| **57** | 52.25 | T | F | T | HCCH | 70.00 | F | T | T | CCCC | √ | | √ | | | √ |
| **58** | 63.25 | T | T | N/A | HCCH | 63.25 | T | T | N/A | HCCH | | √ | | √ | | √ |
| **59** | 22.75 | T | T | F | HCCH | 22.75 | T | T | F | HCCH | | √ | | √ | | √ |
| **60** | 62.50 | T | T | N/A | N/A | 67.50 | F | F | T | N/A | | √ | | √ | √ | |
| **Average** | **56.9** | | | | | **63.7** | | | | **Sum** | **31** | **29** | **36** | **23** | **31** | **26** |
| **Time shift from hopping to decision time = 6.8 fs** | | | | | | | | | | **%** | **52** | **48** | **61** | **39** | **54** | **46** |

| | | | | | | | | | | |
|---|---|---|---|---|---|---|---|---|---|---|
| | | **leading mode** | **HCCH (HOOP works)** | **39-41** | | **leading mode** | **HCCH** | **41-43** | | |
| | | | **CCCC** | **12-14** | | | **CCCC** | **9-11** | | |
| | | | **N/A** | **7** | | | **N/A** | **8** | | |
| | | | **HOOP breaks (or N/A)** | **18** | | | **HOOP breaks (or N/A)** | **12-15** | | |
| | | | **HCCH breaks (or N/A)** | **10** | | | **HCCH breaks (or N/A)** | **10-12** | | |

*where T refers to the trajectory in which the direction of the mode is in line with the computed photoproduct, F is opposite to T while N/A refers to the cases at which the direction is not clear or at turning point. The decision time is the time at which the WF is changed to a biradical one. The leading mode is the one which exhibits the largest deformation at the hopping/decision times, the average hopping time and τ (defined as the time period it takes for half of the population to decay to the GS) are roughly identical. The assignment in each trajectory is carried out using the specific figure for $HC_{11}C_{12}H$, HOOP, $CC_{11}C_{12}C$ and charges on N-moiety given in **Figure S10**.

**Table S8***. Statistical analysis of the individual trajectories of the sqRh ensemble showing the hopping/decision times, the direction of the $HC_{11}C_{12}H$, HOOP, $CC_{11}C_{12}C$ and the leading modes, and the computed and expected photoproduct distributions at both hopping/decision times.

| Traj | hopping time (fs) | Product formation follows … | | | leading mode | decision time (fs) | Product formation follows … | | | leading mode | Computed Product | | Expected Product at hopping time | | Expected Product at decision time | |
|---|---|---|---|---|---|---|---|---|---|---|---|---|---|---|---|---|
| | | $HC_{11}$-$C_{12}H$ at hopping time | HOOP at hopping time | $CC_{11}C_{12}C$ at hopping time | | | $HC_{11}C_{12}H$ at decision time | HOOP at decision time | $CC_{11}C_{12}C$ at decision time | | Trans | Cis | Trans | Cis | Trans | Cis |
| **01** | 53.00 | T | T | F | HCCH | 64.50 | T | T | F | HCCH | | √ | | √ | | √ |
| **02** | 50.00 | T | N/A | T | CCCC | 61.25 | T | T | T | HCCH/CCCC | √ | | √ | | √ | |
| **03** | 58.50 | T | F | T | CCCC | 58.50 | T | F | T | CCCC | √ | | √ | | √ | |
| **04** | 54.00 | T | T | T | HCCH | 54.00 | T | T | T | HCCH | √ | | √ | | √ | |
| **05** | 59.00 | T | T | F | HCCH | 74.00 | T | T | N/A | HCCH | | √ | | √ | | √ |
| **06** | 36.00 | F | F | T | N/A | 49.00 | T | T | N/A | HCCH | √ | | | √ | √ | |
| **07** | 40.00 | T | T | T | HCCH | 58.25 | T | T | N/A | HCCH | √ | | √ | | √ | |
| **08** | 52.50 | T | T | T | HCCH | 64.00 | T | T | T | HCCH | √ | | √ | | √ | |
| **09** | 63.50 | T | T | N/A | HCCH | 78.00 | T | F | T | CCCC | | √ | | √ | | √ |
| **10** | 50.75 | T | T | T | HCCH | 62.00 | T | T | T | HCCH | √ | | √ | | √ | |
| **11** | 63.75 | F | F | T | N/A | 63.75 | F | F | T | N/A | √ | | | √ | | √ |
| **12** | 81.75 | T | T | F | HCCH | 97.75 | T | N/A | T | CCCC | | √ | | √ | | √ |
| **13** | 44.75 | F | F | N/A | N/A | 58.00 | T | T | N/A | HCCH | | √ | √ | | | √ |
| **14** | 44.00 | T | T | N/A | HCCH | 56.25 | T | T | N/A | HCCH | √ | | √ | | √ | |
| **15** | 62.50 | F | F | T | N/A | 62.50 | F | F | T | N/A | √ | | | √ | | √ |
| **16** | 63.50 | T | T | N/A | HCCH | 77.25 | T | F | T | CCCC | | √ | | √ | | √ |
| **17** | 103.00 | T | T | F | HCCH | 113.50 | N/A | F | T | CCCC | √ | | √ | | - | |
| **18** | 32.25 | F | T | F | N/A | 32.25 | F | T | F | HCCH/CCCC | | √ | √ | | √ | |
| **19** | 56.75 | N/A | F | T | CCCC | 68.25 | T | N/A | T | HCCH | √ | | - | | √ | |
| **20** | 66.25 | F | F | T | N/A | 66.25 | F | F | T | N/A | √ | | | √ | | √ |
| **21** | 39.75 | T | T | F | HCCH | 54.25 | T | T | T | HCCH | | √ | | √ | | √ |
| **22** | 83.50 | T | T | N/A | HCCH | 83.50 | T | T | N/A | HCCH | √ | | √ | | √ | |
| **23** | 72.25 | T | N/A | T | CCCC | 92.50 | T | T | T | HCCH | | √ | | √ | | √ |
| **24** | 60.75 | T | T | T | HCCH | 60.75 | T | T | T | HCCH | √ | | √ | | √ | |
| **25** | 38.75 | T | F | T | CCCC | **90.00** | F | T | T | CCCC | √ | | √ | | √ | |
| **26** | 51.25 | T | T | T | HCCH | 56.00 | T | T | T | HCCH | √ | | √ | | √ | |
| **27** | 55.25 | F | F | T | CCCC | 66.00 | T | T | T | HCCH | √ | | | √ | √ | |
| **28** | 48.00 | T | T | T | HCCH | 48.00 | T | T | T | HCCH | √ | | √ | | √ | |
| **29** | 49.00 | F | F | N/A | N/A | 49.00 | F | F | N/A | N/A | √ | | | √ | | √ |
| **30** | 48.75 | T | T | T | HCCH | 63.00 | T | T | T | HCCH | √ | | √ | | √ | |
| **31** | 57.00 | T | T | N/A | HCCH | 57.00 | T | T | N/A | HCCH | | √ | | √ | | √ |
| **32** | 43.75 | T | T | N/A | HCCH | 43.75 | T | T | N/A | HCCH | √ | | √ | | √ | |
| **33** | 75.25 | F | F | N/A | N/A | 115.00 | T | T | T | HCCH | √ | | | √ | √ | |
| **34** | 56.75 | F | T | F | HCCH | 68.50 | T | T | N/A | HCCH | | √ | √ | | | √ |
| **35** | 26.50 | F | F | T | CCCC | 49.50 | T | T | T | HCCH | √ | | | √ | √ | |
| **36** | 72.50 | T | T | T | HCCH | 84.50 | T | T | T | HCCH | √ | | √ | | √ | |

**Continue Table S8**

| Traj | hopping time (fs) | Product formation follows … | | | leading mode | decision time (fs) | Product formation follows … | | | leading mode | Computed Product | | Expected Product at hopping time | | Expected Product at decision time | |
|---|---|---|---|---|---|---|---|---|---|---|---|---|---|---|---|---|
| | | $HC_{11}$-$C_{12}H$ at hopping time | HOOP at hopping time | $CC_{11}C_{12}C$ at hopping time | | | $HC_{11}C_{12}H$ at decision time | HOOP at decision time | $CC_{11}C_{12}C$ at decision time | | Trans | Cis | Trans | Cis | Trans | Cis |
| **37** | 62.50 | T | T | F | HCCH | 62.50 | T | T | F | HCCH | | √ | | √ | | √ |
| **38** | 56.25 | F | F | T | N/A | 56.25 | F | F | T | N/A | √ | | | √ | | √ |
| **39** | 74.25 | T | F | T | CCCC | 102.25 | T | T | T | HCCH | √ | | √ | | √ | |
| **40** | 58.25 | T | T | F | N/A | 82.75 | F | F | T | N/A | | √ | √ | | √ | |
| **41** | 107.25 | T | T | F | HCCH | 134.50 | T | T | T | HCCH/CCCC | | √ | | √ | | √ |
| **42** | 60.75 | T | F | T | CCCC | 60.75 | T | F | T | CCCC | √ | | √ | | √ | |
| **43** | 51.00 | T | T | T | HCCH | 51.00 | T | T | T | HCCH | √ | | √ | | √ | |
| **44** | 37.50 | T | T | T | HCCH | 48.75 | T | T | T | HCCH | √ | | √ | | √ | |
| **45** | 49.75 | N/A | F | T | HCCH | 49.75 | T | T | T | HCCH | √ | | - | | √ | |
| **46** | 73.50 | T | T | N/A | HCCH | 80.50 | T | T | N/A | HCCH | √ | | √ | | √ | |
| **47** | 94.50 | T | T | F | HCCH | 94.50 | T | T | F | HCCH | | √ | √ | √ | | √ |
| **48** | 60.50 | N/A | T | T | HCCH | 74.50 | T | T | T | HCCH | √ | | - | | √ | |
| **49** | 58.00 | T | T | F | HCCH | 58.00 | T | T | F | HCCH | | √ | | √ | | √ |
| **50** | 62.50 | T | T | T | HCCH | 62.50 | T | T | T | HCCH | | √ | √ | | √ | |
| **51** | 65.75 | T | T | N/A | HCCH | 65.75 | T | T | N/A | HCCH | √ | | √ | | √ | |
| **52** | 81.75 | T | T | T | HCCH | 96.50 | T | T | T | HCCH | √ | | √ | | √ | |
| **53** | 56.00 | T | T | T | HCCH | 67.25 | T | T | T | HCCH | √ | | √ | | √ | |
| **54** | 69.25 | F | F | T | N/A | 69.25 | F | F | T | N/A | | √ | √ | | √ | |
| **55** | 85.75 | T | T | T | HCCH | 85.75 | T | T | T | HCCH | √ | | √ | | √ | |
| **56** | 45.75 | T | T | T | HCCH | 54.75 | T | T | T | HCCH | √ | | √ | | √ | |
| **57** | 57.00 | T | T | T | HCCH | 72.00 | T | T | T | CCCC | √ | | √ | | √ | |
| **58** | 45.25 | T | T | T | HCCH | 45.25 | T | T | T | HCCH | √ | | √ | | √ | |
| **59** | 57.00 | F | F | N/A | N/A | 76.50 | T | T | T | HCCH | | √ | √ | | | √ |
| **60** | 50.00 | T | T | T | HCCH | 50.00 | T | T | T | HCCH | √ | | √ | | √ | |
| **Average** | **58.9** | | | | | **68.4** | | | | **Sum** | **41** | **19** | **37** | **21** | **39** | **20** |
| **Time shift from hopping to decision time = 9.5 fs** | | | | | | | | | | **%** | **68** | **32** | **64** | **36** | **66** | **34** |

| | | | | | | | | | | |
|---|---|---|---|---|---|---|---|---|---|---|
| | | | **HCCH (HOOP works)** | **39** | | | **HCCH (HOOP works)** | **42-45** | | |
| | | **leading mode** | **CCCC** | **9** | | **leading mode** | **CCCC** | **8-11** | | |
| | | | **N/A** | **12** | | | **N/A** | **7** | | |
| | | | **HOOP breaks (or N/A)** | **20** | | | **HOOP breaks (or N/A)** | **14** | | |
| | | | **HCCH breaks (or N/A)** | **17** | | | **HCCH breaks (or N/A)** | **10** | | |

*where T refers to the trajectory in which the direction of the mode is in line with the computed photoproduct, F is opposite to T while N/A refers to the cases at which the direction is not clear or at turning point. The decision time is the time at which the WF is changed to a biradical one. The leading mode is the one which exhibits the largest deformation at the hopping/decision times, the average hopping time and τ (defined as the time period it takes for half of the population to decay to the GS) are roughly identical. The assignment in each trajectory is carried out using the specific figure for $HC_{11}C_{12}H$, HOOP, $CC_{11}C_{12}C$ and charges on N-moiety given in **Figure S11**.

**Table S9***. Statistical analysis of the individual trajectories of the Rh ensemble showing the hopping /decision times, the direction of the $HC_{11}C_{12}H$, HOOP, $CC_{11}C_{12}C$ and the leading modes, and the computed and expected photoproduct distributions at both hopping/decision times.

| Traj | hopping time (fs) | Product formation follows … | | | leading mode | decision time (fs) | Product formation follows … | | | leading mode | Computed Product | | Expected Product at hopping time | | Expected Product at decision time | |
|---|---|---|---|---|---|---|---|---|---|---|---|---|---|---|---|---|
| | | $HC_{11}$-$C_{12}H$ at hopping time | HOOP at hopping time | $CC_{11}C_{12}C$ at hopping time | | | $HC_{11}C_{12}H$ at decision time | HOOP at decision time | $CC_{11}C_{12}C$ at decision time | | Trans | Cis | Trans | Cis | Trans | Cis |
| **01** | 88.50 | F | F | F | N/A | 90.00 | T | T | F | HCCH | | √ | √ | | | √ |
| **02** | 49.50 | F | F | N/A | N/A | 66.50 | T | T | N/A | HCCH | | √ | √ | | | √ |
| **03** | 62.50 | T | T | N/A | HCCH | 62.50 | T | T | N/A | HCCH | √ | | √ | | √ | |
| **04** | 83.50 | T | T | N/A | HCCH | 86.25 | T | T | N/A | HCCH | | √ | | √ | | √ |
| **05** | 108.75 | T | T | N/A | HCCH | 108.75 | T | T | N/A | HCCH | √ | | √ | | √ | |
| **06** | 77.25 | T | F | T | CCCC | 94.50 | T | T | N/A | HCCH | √ | | √ | | √ | |
| **07** | 68.00 | T | F | T | CCCC | 68.00 | T | F | T | CCCC | √ | | √ | | √ | |
| **08** | 91.75 | T | T | T | HCCH | 91.75 | T | T | T | HCCH | √ | | √ | | √ | |
| **09** | 107.75 | T | T | F | HCCH | 114.75 | T | T | T | HCCH | √ | | √ | | √ | |
| **10** | 76.50 | T | T | N/A | HCCH | 76.50 | T | T | N/A | HCCH | √ | | √ | | √ | |
| **11** | 126.00 | T | T | T | HCCH | 126.00 | T | T | T | HCCH | √ | | √ | | √ | |
| **12** | 97.75 | T | T | T | HCCH | 97.75 | T | T | T | HCCH | | √ | | √ | | √ |
| **13** | 89.00 | T | N/A | T | CCCC | 108.50 | T | T | T | HCCH | √ | | √ | | √ | |
| **14** | 75.25 | F | F | T | CCCC | 86.75 | T | T | N/A | HCCH | √ | | | √ | √ | |
| **15** | 172.25 | T | T | T | HCCH | 189.75 | T | N/A | T | HCCH | | √ | | √ | | √ |
| **16** | 49.25 | T | T | F | HCCH | 66.00 | T | N/A | T | HCCH | √ | | √ | | √ | |
| **17** | 112.25 | N/A | N/A | T | CCCC | 120.25 | N/A | F | T | CCCC | | √ | - | | - | |
| **18** | 50.25 | T | T | T | HCCH | 59.75 | T | T | T | HCCH | √ | | √ | | √ | |
| **19** | 85.50 | T | T | T | HCCH | 85.50 | T | T | T | HCCH | √ | | √ | | √ | |
| **20** | 56.50 | T | T | F | HCCH | 67.25 | T | T | F | HCCH | | √ | | √ | | √ |
| **21** | 81.50 | N/A | F | T | CCCC | 93.00 | T | T | T | HCCH | √ | | - | | √ | |
| **22** | 59.75 | F | F | N/A | N/A | 72.50 | T | T | T | HCCH | | √ | √ | | | √ |
| **23** | 97.50 | T | T | T | HCCH | 97.50 | T | T | T | HCCH | √ | | √ | | √ | |
| **24** | 82.25 | T | T | N/A | HCCH | 82.25 | T | T | N/A | HCCH | √ | | √ | | √ | |
| **25** | 77.50 | T | T | T | HCCH | 77.50 | T | T | T | HCCH | √ | | √ | | √ | |
| **26** | 82.75 | T | T | F | HCCH | 91.50 | T | T | T | HCCH | | √ | | √ | | √ |
| **27** | 44.75 | F | F | F | N/A | 54.25 | T | T | F | HCCH | | √ | √ | | | √ |
| **28** | 61.50 | T | T | T | HCCH | 61.50 | T | T | T | HCCH | √ | | √ | | √ | |
| **29** | 58.25 | T | T | F | HCCH | 67.50 | T | T | F | HCCH | | √ | | √ | | √ |
| **30** | 69.75 | T | T | T | HCCH | 69.75 | T | T | T | HCCH | √ | | √ | | √ | |
| **31** | 75.75 | T | T | N/A | HCCH | 93.25 | T | T | N/A | HCCH | √ | | √ | | √ | |
| **32** | 63.00 | T | T | F | HCCH | 63.00 | T | T | F | HCCH | | √ | | √ | | √ |
| **33** | 86.25 | T | T | F | HCCH | 86.25 | T | T | F | HCCH | | √ | | √ | | √ |
| **34** | 44.00 | T | T | T | HCCH | 44.00 | T | T | T | HCCH | √ | | √ | | √ | |
| **35** | 80.00 | T | T | T | HCCH | 80.00 | T | T | T | HCCH | √ | | √ | | √ | |
| **36** | 48.75 | T | T | T | HCCH | 48.75 | T | T | T | HCCH | √ | | √ | | √ | |

**Continue Table S9**

| Traj | hopping time (fs) | Product formation follows … | | | leading mode | decision time (fs) | Product formation follows … | | | leading mode | Computed Product | | Expected Product at hopping time | | Expected Product at decision time | |
|---|---|---|---|---|---|---|---|---|---|---|---|---|---|---|---|---|
| | | $HC_{11}$-$C_{12}H$ at hopping time | HOOP at hopping time | $CC_{11}C_{12}C$ at hopping time | | | $HC_{11}C_{12}H$ at decision time | HOOP at decision time | $CC_{11}C_{12}C$ at decision time | | Trans | Cis | Trans | Cis | Trans | Cis |
| **37** | 90.50 | T | T | N/A | HCCH | 90.50 | T | T | N/A | HCCH | √ | | √ | | √ | |
| **38** | 83.25 | T | T | T | HCCH | 83.25 | T | T | T | HCCH | √ | | √ | | √ | |
| **39** | 44.50 | T | T | T | N/A | 56.00 | T | T | T | HCCH | √ | | √ | | √ | |
| **40** | 100.75 | T | T | T | HCCH | 100.75 | T | T | T | HCCH | √ | | √ | | √ | |
| **41** | 85.25 | T | T | T | HCCH | 85.25 | T | T | T | HCCH | √ | | √ | | √ | |
| **42** | 85.50 | T | T | F | HCCH | 85.50 | T | T | F | HCCH | √ | | √ | | √ | |
| **43** | 73.75 | T | T | N/A | HCCH | 73.75 | T | T | N/A | HCCH | √ | | √ | | √ | |
| **44** | 76.25 | T | T | T | HCCH | 76.25 | T | T | T | HCCH | √ | | √ | | √ | |
| **45** | 77.50 | T | T | T | HCCH | 87.25 | T | T | T | HCCH | √ | | √ | | √ | |
| **46** | 74.00 | T | T | T | HCCH | 83.00 | T | T | T | HCCH | √ | | √ | | √ | |
| **47** | 100.75 | T | T | T | HCCH | 111.75 | T | T | T | HCCH | √ | | √ | | √ | |
| **48** | 85.75 | T | N/A | T | HCCH/CCCC | 85.75 | T | N/A | T | HCCH/CCCC | √ | | √ | | √ | |
| **49** | 69.50 | T | T | F | HCCH | 69.50 | T | T | F | HCCH | | √ | | √ | | √ |
| **50** | 65.75 | T | T | T | HCCH | 65.75 | T | T | T | HCCH | √ | | √ | | √ | |
| **51** | 96.00 | T | T | N/A | HCCH | 115.00 | F | F | T | CCCC | √ | | √ | | | √ |
| **52** | 69.00 | T | F | F | N/A | 76.75 | T | T | F | HCCH | | √ | | √ | | √ |
| **53** | 65.75 | T | T | T | HCCH | 65.75 | T | T | T | HCCH | √ | | √ | | √ | |
| **54** | 57.00 | T | T | T | HCCH | 65.00 | T | T | T | HCCH/CCCC | √ | | √ | | √ | |
| **55** | 88.50 | T | T | F | HCCH | 103.00 | T | T | T | HCCH | √ | | √ | | √ | |
| **56** | 135.00 | T | T | N/A | HCCH/N/A | 135.00 | T | T | N/A | HCCH/N/A | | √ | | √ | | √ |
| **57** | 90.25 | T | T | T | HCCH | 90.25 | T | T | T | HCCH | √ | | √ | | √ | |
| **58** | 56.50 | T | T | F | HCCH | 69.25 | T | F | T | CCCC | | √ | | √ | | √ |
| **59** | 46.75 | F | F | N/A | N/A | 63.00 | T | T | T | HCCH | | √ | √ | | | √ |
| **60** | 79.25 | T | T | T | HCCH | 92.25 | T | T | T | HCCH | √ | | √ | | √ | |
| **Average** | **79.0** | | | | | **84.7** | | | | **Sum** | **42** | **18** | **45** | **13** | **41** | **18** |
| **Time shift from hopping to decision time = 5.7 fs** | | | | | | | | | | **%** | **70** | **30** | **78** | **22** | **69** | **31** |

| | | | | | | | | | | | |
|---|---|---|---|---|---|---|---|---|---|---|---|
| | | **leading mode** | **HCCH (HOOP works)** | | **45-47** | | **leading mode** | **HCCH** | | **53-56** | |
| | | | **CCCC** | | **7-7** | | | **CCCC** | | **4-6** | |
| | | | **N/A** | | **7-8** | | | **N/A** | | **0-1** | |
| | | | **HOOP breaks (or N/A)** | | **13** | | | **HOOP breaks (or N/A)** | | **7** | |
| | | | **HCCH breaks (or N/A)** | | **8** | | | **HCCH breaks (or N/A)** | | **2** | |

*where T refers to the trajectory in which the direction of the mode is in line with the computed photoproduct, F is opposite to T while N/A refers to the cases at which the direction is not clear or at turning point. The decision time is the time at which the WF is changed to a biradical one. The leading mode is the one which exhibits the largest deformation at the hopping/decision times, the average hopping time and τ (defined as the time period it takes for half of the population to decay to the GS) are roughly identical. The assignment in each trajectory is carried out using the specific figure for $HC_{11}C_{12}H$, HOOP, $CC_{11}C_{12}C$ and charges on N-moiety given in the **Figure S12**.

# 9 References:


1. Murakami, M.; Kouyama, T., Crystal structure of squid rhodopsin. *Nature* **2008,** *453* (7193), 363-367.
2. Rinaldi, S.; Melaccio, F.; Gozem, S.; Fanelli, F.; Olivucci, M., Comparison of the isomerization mechanisms of human melanopsin and invertebrate and vertebrate rhodopsins. *Proceedings of the National Academy of Sciences* **2014,** *111* (5), 1714-1719.
3. Okada, T.; Sugihara, M.; Bondar, A.-N.; Elstner, M.; Entel, P.; Buss, V., The Retinal Conformation and its Environment in Rhodopsin in Light of a New 2.2 Å Crystal Structure†. *J. Mol. Biol.* **2004,** *342* (2), 571-583.
4. Punwong, C.; Owens, J.; Martínez, T. J., Direct QM/MM Excited-State Dynamics of Retinal Protonated Schiff Base in Isolation and Methanol Solution. *The journal of physical chemistry. B* **2015,** *119* (3), 704-714.
5. Sekharan, S.; Altun, A.; Morokuma, K., QM/MM Study of Dehydro and Dihydro β-Ionone Retinal Analogues in Squid and Bovine Rhodopsins: Implications for Vision in Salamander Rhodopsin. *Journal of the American Chemical Society* **2010,** *132* (45), 15856-15859.
6. Senn, H. M.; Thiel, W., QM/MM methods for biomolecular systems. *Angewandte Chemie (International ed. in English)* **2009,** *48* (7), 1198-229.
7. Lin, H.; Truhlar, D. G., QM/MM: what have we learned, where are we, and where do we go from here? *Theoretical Chemistry Accounts* **2007,** *117* (2), 185.
8. Altoè, P.; Stenta, M.; Bottoni, A.; Garavelli, M., A tunable QM/MM approach to chemical reactivity, structure and physico-chemical properties prediction. *Theor. Chem. Acc.* **2007,** *118* (1), 219-240.
9. Roos, B.; Taylor, P. R.; Siegbahn, P. E. M., A complete active space SCF method (CASSCF) using a density matrix formulated super-CI approach. *Chem. Phys.* **1980,** *48* (2), 157-173.
10. Ferré, N.; Olivucci, M., Probing the Rhodopsin Cavity with Reduced Retinal Models at the CASPT2//CASSCF/AMBER Level of Theory. *J. Am. Chem. Soc.* **2003,** *125* (23), 6868-6869.
11. Ferré, N.; Cembran, A.; Garavelli, M.; Olivucci, M., Complete-active-space self-consistent-field/Amber parameterization of the Lys296–retinal–Glu113 rhodopsin chromophore-counterion system. *Theor. Chem. Acc.* **2004,** *112* (4), 335-341.
12. Andersson, K.; Malmqvist, P. A.; Roos, B. O.; Sadlej, A. J.; Wolinski, K., Second-order perturbation theory with a CASSCF reference function. *J. Phys. Chem.* **1990,** *94* (14), 5483-5488.
13. Bonvicini, A.; Demoulin, B.; Altavilla, S. F.; Nenov, A.; El-Tahawy, M. M. T.; Segarra-Martí, J.; Giussani, A.; Batista, V. S.; Garavelli, M.; Rivalta, I., Ultraviolet vision: photophysical properties of the unprotonated retinyl Schiff base in the Siberian hamster cone pigment. *Theor. Chem. Acc.* **2016,** *135* (4), 1-10.
14. El-Tahawy, M. M. T.; Nenov, A.; Garavelli, M., Photoelectrochromism in the Retinal Protonated Schiff Base Chromophore: Photoisomerization Speed and Selectivity under a Homogeneous Electric Field at Different Operational Regimes. *J. Chem. Theory Comput.* **2016,** *12* (9), 4460-4475.
15. Forsberg, N.; Malmqvist, P.-Å., Multiconfiguration perturbation theory with imaginary level shift. *Chem. Phys. Lett.* **1997,** *274* (1-3), 196-204.
16. Ghigo, G.; Roos, B. O.; Malmqvist, P.-Å., A modified definition of the zeroth-order Hamiltonian in multiconfigurational perturbation theory (CASPT2). *Chem. Phys. Lett.* **2004,** *396* (1-3), 142-149.
17. Demoulin, B.; El-Tahawy, M. M. T.; Nenov, A.; Garavelli, M.; Le Bahers, T., Intramolecular photo-induced charge transfer in visual retinal chromophore mimics: electron density-based indices at the TD-DFT and post-HF levels. *Theor. Chem. Acc.* **2016,** *135* (4), 1-10.
18. Cembran, A.; Gonzalez-Luque, R.; Altoe, P.; Merchan, M.; Bernardi, F.; Olivucci, M.; Garavelli, M., Structure, spectroscopy, and spectral tuning of the gas-phase retinal chromophore: the beta-ionone "handle" and alkyl group effect. *J. Phys. Chem. A* **2005,** *109* (29), 6597-605.

19. Rivalta, I.; Nenov, A.; Weingart, O.; Cerullo, G.; Garavelli, M.; Mukamel, S., Modelling Time-Resolved Two-Dimensional Electronic Spectroscopy of the Primary Photoisomerization Event in Rhodopsin. *J. Phys. Chem. B* **2014,** *118* (28), 8396-8405.
20. Polli, D.; Altoe, P.; Weingart, O.; Spillane, K. M.; Manzoni, C.; Brida, D.; Tomasello, G.; Orlandi, G.; Kukura, P.; Mathies, R. A.; Garavelli, M.; Cerullo, G., Conical intersection dynamics of the primary photoisomerization event in vision. *Nature* **2010,** *467* (7314), 440-443.
21. Frutos, L. M.; Andruniow, T.; Santoro, F.; Ferre, N.; Olivucci, M., Tracking the excited-state time evolution of the visual pigment with multiconfigurational quantum chemistry. *Proc. Natl. Acad. Sci. U. S. A.* **2007,** *104* (19), 7764-9.
22. Sloane, C. S.; Hase, W. L., On the dynamics of state selected unimolecular reactions: Chloroacetylene dissociation and predissociation. *The Journal of Chemical Physics* **1977,** *66* (4), 1523-1533.
23. Swope, W. C.; Andersen, H. C.; Berens, P. H.; Wilson, K. R., A computer simulation method for the calculation of equilibrium constants for the formation of physical clusters of molecules: Application to small water clusters. *J. Chem. Phys.* **1982,** *76* (1), 637-649.
24. Granucci, G.; Persico, M., Critical appraisal of the fewest switches algorithm for surface hopping. *J. Chem. Phys.* **2007,** *126* (13), 134114.
25. Werner, H.-J.; Knowles, P.; Lindh, R.; Manby, F. R.; Schütz, M.; Celani, P.; Korona, T.; Rauhut, G.; Amos, R.; Bernhardsson, A., MOLPRO, version 2010.1, a package of ab initio programs. *See http://www. molpro. net* **2010**.
26. Aquilante, F.; De Vico, L.; Ferré, N.; Ghigo, G.; Malmqvist, P.-å.; Neogrády, P.; Pedersen, T. B.; Pitoňák, M.; Reiher, M.; Roos, B. O.; Serrano-Andrés, L.; Urban, M.; Veryazov, V.; Lindh, R., MOLCAS 7: The Next Generation. *J. Comput. Chem.* **2009,** *31* (1), 224-247.
27. Aquilante, F.; Autschbach, J.; Carlson, R. K.; Chibotaru, L. F.; Delcey, M. G.; De Vico, L.; Fdez. Galván, I.; Ferré, N.; Frutos, L. M.; Gagliardi, L.; Garavelli, M.; Giussani, A.; Hoyer, C. E.; Li Manni, G.; Lischka, H.; Ma, D.; Malmqvist, P. Å.; Müller, T.; Nenov, A.; Olivucci, M.; Pedersen, T. B.; Peng, D.; Plasser, F.; Pritchard, B.; Reiher, M.; Rivalta, I.; Schapiro, I.; Segarra-Martí, J.; Stenrup, M.; Truhlar, D. G.; Ungur, L.; Valentini, A.; Vancoillie, S.; Veryazov, V.; Vysotskiy, V. P.; Weingart, O.; Zapata, F.; Lindh, R., Molcas 8: New capabilities for multiconfigurational quantum chemical calculations across the periodic table. *J. Comput. Chem.* **2016,** *37* (5), 506-541.
28. Garavelli, M.; Celani, P.; Bernardi, F.; Robb, M. A.; Olivucci, M., The C5H6NH2+ Protonated Shiff Base: An ab Initio Minimal Model for Retinal Photoisomerization. *Journal of the American Chemical Society* **1997,** *119* (29), 6891-6901.
29. Matsuyama, T.; Yamashita, T.; Imamoto, Y.; Shichida, Y., Photochemical properties of mammalian melanopsin. *Biochemistry* **2012,** *51* (27), 5454-62.
30. Suzuki, T.; Uji, K.; Kito, Y., Studies on cephalopod rhodopsin: photoisomerization of the chromophore. *Biochimica et biophysica acta* **1976,** *428* (2), 321-38.
31. Hurley, J. B.; Ebrey, T. G.; Honig, B.; Ottolenghi, M., Temperature and wavelength effects on the photochemistry of rhodopsin, isorhodopsin, bacteriorhodopsin and their photoproducts. *Nature* **1977,** *270*, 540.
32. Tomasello, G.; Olaso-González, G.; Altoè, P.; Stenta, M.; Serrano-Andrés, L.; Merchán, M.; Orlandi, G.; Bottoni, A.; Garavelli, M., Electrostatic Control of the Photoisomerization Efficiency and Optical Properties in Visual Pigments: On the Role of Counterion Quenching. *Journal of the American Chemical Society* **2009,** *131* (14), 5172-5186.
33. Cembran, A.; Bernardi, F.; Olivucci, M.; Garavelli, M., The retinal chromophore/chloride ion pair: Structure of the photoisomerization path and interplay of charge transfer and covalent states. *Proceedings of the National Academy of Sciences of the United States of America* **2005,** *102* (18), 6255-6260.
34. Gozem, S.; Luk, H. L.; Schapiro, I.; Olivucci, M., Theory and Simulation of the Ultrafast Double-Bond Isomerization of Biological Chromophores. *Chemical Reviews* **2017**.

35. Hurley, J. B.; Ebrey, T. G.; Honig, B.; Ottolenghi, M., Temperature and wavelength effects on the photochemistry of rhodopsin, isorhodopsin, bacteriorhodopsin and their photoproducts. *Nature* **1977,** *270* (5637), 540-542.